REVIEWS in MINERALOGY Volume 31

Chapter 9

Chemical Weathering Rates of Silicate Minerals

Editors:

Arthur F. White
U.S. Geological Survey, Menlo Park, CA

Susan L. Brantley
Pennsylvania State University

Front cover: Denticulated margin on naturally weathered hornblende formed by side-by-side coalescence of lenticular etch pits. From a weathered corestone developed on the Carroll Knob Complex in the Appalachian Blue Ridge near Otto, North Carolina. Field of view = 60 μm wide. Courtesy of M.A. Velbel, Michigan State University. See Velbel (1993) *American Mineralogist* 78:405-414.

Back Cover: SEM image of a naturally weathered (001) cleavage surface of an alkali feldspar from gravels formed from the granite at Shap, northern England. Scale bar: 2 μm. The paired triangular and trapezoidal etch pits have developed at the outcrop of edge dislocations. These form extended loops around perthitic albite lamellae in orthoclase. The lamellae extend parallel to *b*, the long axis of the micrograph. Courtesy of M.R. Lee and I. Parsons (see Chapter 8).

Series Editor: **Paul H. Ribbe**
Department of Geological Sciences
Virginia Polytechnic Institute & State University
Blacksburg, Virginia 24061 U.S.A.

Mineralogical Society of America
Washington, D.C.

Chapter 9

CHEMICAL WEATHERING RATES OF SILICATE MINERALS IN SOILS

Art F. White

U. S. Geological Survey
Menlo Park, CA 94025 U.S.A.

INTRODUCTION

Soil can be defined as "a natural body consisting of generally unconsolidated layers or horizons of mineral and/or organic constituents of variable thickness which differ from parent-rock in morphological, physical, chemical and mineralogical properties" (Joffe, 1949). As such, the study of soils have long been tied to the nature and extent of chemical weathering. The literature on soil chemical weathering related to secondary mineralogy, chemical equilibrium and ion exchange, in addition to the effects on geomorphology and other physical processes, has been reviewed in a number of books (Lindsay, 1979; Nahon, 1991; Sparks and Suarez, 1991; and Sposito, 1994). The present review discusses the rates of chemical weathering of primary silicate minerals in soil environments. Although soils represent one of the most accessible natural environments, relatively few studies have quantitatively addressed weathering rates of feldspars, amphiboles, pyroxenes, micas and other silicate minerals under such conditions. Estimating weathering rates of silicate minerals in soils is important because such reactions ultimately control rates of soil development and secondary mineral formation. Weathering rates also influence soil buffering capacities related to acidic deposition in watersheds and control the cycling of many inorganic nutrients which are important in soil fertility and carbon cycling.

The chemical weathering of a primary mineral j in a soil can be defined in simplest terms as

$$M_j = k_j S \Delta t \quad (1)$$

were M_j is the mass loss (mol), k_j is the rate constant (mol cm^{-2} s^{-1}), S is the surface area (cm^2) and Δt the time period (s) during which weathering occurred. These terms, as well others used throughout the paper, are tabulated in Table 1. In weathering studies of natural systems, Equation (1) can be employed as a predictive tool to determine any one of the above parameters provided that the other terms are known. The present paper will discuss methods used to determine mass losses, surface areas and duration of weathering, which in turn, will permit calculation of weathering rate constants for soil environments.

Chemical weathering of primary silicates in soils will be addressed in the present paper from two perspectives. These will be (a) rates determined from solid state element and mineral losses relative to initial or parent material and (b) rates determined from solute fluxes through the soil profile. These parallel approaches require the determination of mass loss M_j based on either mineral or solute compositions. Soil mineralogy represents the residual product of chemical reactions which integrate the weathering rate over the entire period of soil development. In contrast, solute chemistry and fluxes reflect present day weathering under current chemical and hydrologic conditions. Both approaches require the determination of the duration of weathering. In the case of mineral or elemental loses, duration of

Table 1. Summary of parameters referred to in text[1].

Symbol	Definition	Units
a	Rate of etch pit annihilation	s^{-1}
$C_{j,w}$	Concentration of weatherable mineral or element in soil profile	g g^{-1}
$C_{j,p}$	Concentration of weatherable mineral or element in protolith	g g^{-1}
$C_{i,w}$	Concentration of inert mineral or element in soil profile	g g^{-1}
$C_{i,p}$	Concentration of inert mineral or element in protolith	g g^{-1}
C_{qtz}	Concentration of quartz in soil	g g^{-1}
C^*	Concentration of aluminosilicates in soil	g g^{-1}
c_k'	Concentration of solute species k contributed by dissolution	mol cm^{-3}
c_k	Solute concentration measured in soil solution	mol cm^{-3}
c_k^s	Solute concentration incorporated into secondary phases	mol cm^{-3}
c_k^a	Solute concentration contributed from non-weathering sources	mol cm^{-3}
D	Mineral grain diameter	cm
E_a	Activation energy	kJ mol^{-1}
ET	Evapotranspiration	cm
f_m	Mass fraction of mineral in soil	g g^{-1}
f^ϕ	Mass fraction of mineral in size fraction ϕ	g g^{-1}
G	Etch pit growth rate	cm s^{-1}
h_g	Hydraulic head due to gravity flow	cm H_2O
h_p	Hydraulic head related to matrix potential	cm H_2O
IAP	Aqueous activity product for soil solution	
K_m	Unsaturated zone hydraulic conductivity	cm s^{-1}
K	Solubility constant of mineral phase	
k_j	Weathering rate constant for mineral phase j	mol $cm^{-2}.s^{-1}$
M	Mass of soil	g
M_j	Mass of mineral phase reacted	mol
$M^\phi_{j,w}$	Mass of residual mineral in soil	g
$M^\phi_{j,p}$	Mass of mineral in protolith	g
$m_{j,flux}$	Mass flux of mineral weathered	mol cm^{-2}
m	Moisture content of soil	cm^3cm^{-3}
n	Number of etch pits	cm cm^{-2}
$N_{j,k}$	Stoichiometric ratio of species k in mineral phase j	mol mol^{-1}
P	Precipitation	cm
Q_w	Watershed mass flux	g $m^{-2}s^{-1}$
Q_j	Flux of mineral j	mol $cm^2.s$
Q_k	Flux of solute k	mol $cm^2.s$
q	Soil water flux	cm s^{-1}
R	Gas constant	
R_a	Ratio of conservative and weatherable component in soil and parent material	g g^{-1}
R_s	Ratio of unit soil surface area to total surface area of mineral in soil	cm^2 cm^{-2}
r^o	Initial particle radius	cm
r	Final particle radius resulting from weathering	cm
S	Specific mineral surface area	cm^2g^{-1}
S_i	Internal surface area due to porosity	cm^2g^{-1}
S_s	Unit surface area of soil perpendicular to flow	cm^2
S_t	Total surface area of mineral contained in volume of soil	cm^2
s	Geometric mineral surface area	cm^2g^{-1}

T	Temperature	°K
V_p	Volume of protolith	cm^3
V_s	Volume of soil	cm^3
V_j	Molar volume of mineral phase j	$cm^3\ mol^{-1}$
v_p	Volume fraction of saprolite	$cm^3\ cm^{-3}$
v_{in}	Volume fraction of inert minerals in soil	$cm^3\ cm^{-3}$
v_{sec}	Volume fraction of secondary minerals produced in soil	$cm^3\ cm^{-3}$
v_ϕ	Volume fraction of soil attributed to porosity	$cm^3\ cm^{-3}$
W	Etch pit diameter	cm
$x_{qtz,w}$	Mass fraction of quartz in soil	$g\ g^{-1}$
x_w	Mass fraction of weatherable mineral in soil	$g\ g^{-1}$
$x_{qtz,p}$	Mass fraction of quartz in protolith	$g\ g^{-1}$
x_{wp}	Mass fraction of weatherable mineral in protolith	$g\ g^{-1}$
z	Depth of weathering	cm
α	Mineral sphericity	$cm^3\ cm^{-3}$
ΔG_r	Net free energy of reaction	$kJ\ mol^{-1}$
Δt	Time span over which weathering occurs	s
ε_v	Volumetric strain	$cm^3 cm^{-3}$
∇H	Hydraulic gradient	cm H_2O cm^{-1}
A_r	Mineral surface roughness	$cm^2\ cm^{-2}$
A_{ar}	Aluminosilicate surface roughness	$cm^2\ cm^{-2}$
A_{qtz}	Quartz surface roughness	$cm^2\ cm^{-2}$
ρ_p	Density of protolith	$g\ cm^{-3}$
ρ_w	Density of weathered soil	$g\ cm^{-3}$
ρ_j	Density of mineral	$g\ cm^{-3}$
σ	Shear modulus	
τ_w	Transport function describing mass loss from weathering	$g\ g^{-1}$
ω_w	Weathering velocity	$cm\ s^{-1}$
ϕ	Particle size fraction	
θ	Etch pit slope	degree
φ_m	Mineral molecular weight	$mol\ g^{-1}$

Note: To prevent duplication of terms, some original symbols used in cited literature have been changed.

weathering equates to the age of the soil profile. For solutes, the resident time is equivalent to fluid transit time through the soil. Both approaches normalize chemical fluxes to the unit surface area of the mineral phase. A detailed discussion will follow on the definition and role of surface area in weathering rate calculations. Finally, the derived rate constants k_j, based on Equation (1), will be compared for various natural soils and experimental studies. Reasons for observed variations will then be addressed.

WEATHERING ENVIRONMENTS BASED ON SOIL CLASSIFICATION

Weathering rates of primary silicates are strongly influenced by specific soil environments. Due to the complexity of soil weathering and the need to qualitatively describe and compare soil distributions, much effort in soil science has been devoted to methods of soil classification. From the standpoint of weathering, three aspects of soil classifications are relevant.

Soil Profiles: Physical descriptions of soil weathering are dependent on the spatial position or depth in the soil column. Studies often distinguish either explicitly or more often implicitly between a soil profile and a weathering profile (Birkeland, 1984). Where this is

weathering profile. A more inclusive definition of a soil profile is the vertical section that includes all layers that have been pedogenically altered during chemical weathering. Soil horizons defined within such profiles clearly recognize the vertical transition in the degree of weathering from the intensively weathered A and E horizons through the moderately weathered B, to the relatively unaltered C horizons to bedrock (Buol et al., 1989). Such an approach encompasses the entire span of chemical weathering occurring at the earth's surface including both the distribution of primary silicates as well as secondary clay and oxyhydroxide minerals.

Soil Classes: Most of soil science literature is concerned with the upper regions of the soil profile often termed the soil solum. The exact lower boundary of the soil solum is not always defined but is generally shallow (25 to 100 cm) and is the soil profile most influenced by plant roots (Buol and Weed, 1991). Such an emphasis on shallow soil horizons clearly reflects the overriding importance of biological activity in most soil studies as well as the amenability of shallow soils to soil surveys. Modern soil mineral classifications for the major soil orders are based on the description of this shallow zone (Buol et al., 1989). Soil family mineralogy classes are principally oriented toward the distribution of secondary oxyhydroxides and clays in the heavily weathered shallow solum and do not generally include details of the primary silicate distributions more prevalent in deeper soils nor the composition of the underlying bedrock.

Soil Sequences: Soil science attempts to define changes in soil characteristics in terms of specific processes or influences relevant to weathering. Jenny (1980) defined any dependent soil property as a function of a number of independent soil properties or state factors such that

$$Soil\ Property = f\ (pt,\ cl,\ tp,\ t,\ org) \qquad (2)$$

where *pt* is the parent material, *cl* is climate, *tp* is the topography, *t* is the age of the soil and *org* is the role of organisms. Soil sequences can be classified based on a single variable if other conditions effecting soil development are subordinate or relatively constant. Such sequences can be defined as follows:

Lithosequences are series of soils developed on different parent materials or rock types but under similar conditions for other state factors. Differences in parent mineralogy may be the dominant factor determining weathering rates in these soil (Dixon and Weed, 1989). As originally proposed by Goldich (1938), the relative reactivity of minerals decreases in the order: carbonates > mafic silicates > feldspars > quartz. Therefore, the proportions of these primary minerals in a soil profile will strongly influence absolute weathering rates.

Climosequences are soils with similar properties that are influenced principally by differences in precipitation and temperature. An example would include different weathering rates of continuous volcanic ash layers in soils deposited under extreme differences in precipitation conditions on Hawaii (Johnsson et al., 1993).

Toposequences refer to soils formed over lateral variations in slope and topography. Soils at bases of hillslopes or on river flood plains accumulate parent material and have higher moisture contents than upland soils which are non-cumulative and have lower moisture conditions. Such sequences may be important in assessing effects of hydrology and physical versus chemical weathering rates on soil development.

Chronosequences are groups of soils for which all soil forming factors except elapsed time of formation are equivalent. The effect of time on chemical weathering rates is one

explaining many of the observed differences between experimental and natural weathering rates.

Biosequences are soil sequences containing variable biotia such as differences in the extent and type of plant cover. The role of plants in weathering rates is an important issue in soil weathering studies and in deciphering the weathering history of the earth.

Clearly the above soil classifications provide important opportunities to isolate and assess important parameters that influence soil weathering rates.

MINERALOGICAL MASS BALANCES IN SOILS

In the introduction, a soil was defined as being composed of mineral or chemical constituents that differ from the parent material or protolith. As indicated by Equation (1), quantification of the mass difference M_j is required in calculating weathering rates of primary silicates in soils. The following sections discuss the approaches which can been used and the assumptions required to calculate mass losses due to chemical weathering.

Mass Balance Approaches

The simplest approach in determining mineral or chemical losses associated with primary silicates in soils is to determine the ratio of the chemical or mineral concentration j in the weathered soil $C_{j,w}$ to the corresponding concentration in the parent material or protolith $C_{j,p}$ (i.e. $C_{j,w}/C_{j,p}$). However, the mass ratio of mineral or chemical components in soil and parent material is also dependent on concentration and dilution effects caused by the losses and gains of all the other components. The most common method for overcoming this problem is to define the mass ratio in terms of a conservative component i whose absolute mass does not change during weathering of the protolith to form a soil

$$\frac{C_{j,w}}{C_{j,p}} = R_o\left(\frac{C_{i,w}}{C_{i,p}}\right) \tag{3}$$

When $R_o = 1$ the ratio of the weatherable j component equals the ratio of the conservative component i. This signifies that no loss or gain of the j component occurs in the soil and that j also behaves in a conservative fashion during weathering. In contrast, if $R_o = 0$, complete weathering loss of component j occurs. Likewise, the change in volume of a soil relative to the volume of the original parent material can be defined as

$$\frac{V_w}{V_p} = \frac{C_{i,w}}{C_{i,p}} \tag{4}$$

Various forms of Equations (3) and (4) have long been used to estimate the extent of chemical changes in soils (Merrill, 1906; Barth, 1961; Harden, 1987).

A more general approach to soil weathering using the same mass ratios has been developed by Brimhall and Dietrick (1987), Chadwick et al. (1990) and Merritts et al. (1992) where the ratio of the weathered to parent composition is determined by three distinct processes defined on the right hand side of Equation (5).

$$\frac{C_{j,w}}{C_{j,p}} = \frac{\rho_p}{\rho_w}\,\frac{1}{(\epsilon_{j,w} + 1)}\,(1 + \tau_{j,w}) \tag{5}$$

and removal of mobile elements with a corresponding increase in porosity. Volume changes that may be associated with the density changes are described by the strain factor $1/(\epsilon_{j,w}+1)$ where $\epsilon_{j,w} = V_w/V_p - 1$ (Eqn. 4). Together residual enrichment and strain are described as "closed system" contributions which occur without movement of the component under consideration (i.e. $C_{j,w}$). The mass transport component "tau" $\tau_{j,w}$ is an "open system" contribution that describes mass movement across the sample volume boundaries (Brimhall and Dietrick, 1987).

$\tau_{j,w}$ is computed from density and chemical composition data in combination with volume change derived from the strain calculations

$$\tau_{j,w} = \frac{\rho_w C_{j,w}}{\rho_p C_{j,p}} (\epsilon_{j,w} + 1) - 1 \quad (6)$$

When $\tau_{j,w} = -1$, mass of element j was been completely lost during weathering. If $\tau_{j,w} = 0$, the element is immobile and is only affected by internal closed chemical system processes, specially residual and strain effects caused by changes in bulk density and volume. For a truly immobile element i (i.e. $\tau_{j,w} = 0$), Equation (6) can be rearranged to give

$$\epsilon_{j,w} = \frac{\rho_p C_{i,p}}{\rho_w C_{i,w}} - 1 \quad (7)$$

such that the volumetric strain can be calculated. Substitution of Equations (6) and (7) into Equation (5) produces the expected mass transfer relation $\tau_{j,w} = R_o - 1$ (Eqn. 3).

The mass flux resulting from weathering of a volume of soil V_w can be calculated using the open chemical system transport function $\tau_{j,w}$ such that

$$M_j = \left(\rho_p V_w \frac{C_{j,p}}{100} \right) \tau_{j,w} \quad (8)$$

In turn, the overall flux from a soil profile which has undergone variable amounts of mass transfer as a function of depth z can be calculated as

$$M_j = \left(\rho_p \frac{C_{j,p}}{100} \right) \int_{z=0}^{z=d} \tau_{j,w} dz \quad (9)$$

Mass balances are defined in terms of ratios (Eqns. 3 and 5) and are therefore independent of the units employed. Such mass balance calculations are equally applicable to mineral and elemental soil components (White et al., 1995). Equations (8) and (9) are written in terms of mineral concentrations which leads to a direct correlation with the loss of mineral mass M_j in Equation (1). If the above equations are written in terms of elemental concentrations, then M_j must be calculated from mineral stoichiometries.

Required assumptions for mass balance calculations

Two important assumptions concerning mineral and elemental components are required in the mass balance calculations. The first involves determination of the composition of the parent material $C_{j,p}$ prior to the onset of chemical weathering. For soils developed in situ on parent bedrock, such as saprolites, the potential errors in this determination are confined to local heterogeneities in bedrock compositions.

The estimate of the initial composition becomes more difficult when soils are developed on sedimentary parent materials such as alluvial terraces or loess deposits. One approach would be to use the bedrock composition from the assumed source area as the parent material. However for deposits produced by rivers, significant compositional differences can exist between the bedrock in the source area and the downstream sedimentary deposit. This is caused by weathering in upland watersheds coupled with sorting and winnowing during transport and deposition in the rivers. For such deposits, the parent material is commonly assumed to be the least weathered horizon in the soil profile. In practice, this corresponds to the deepest C horizon soils and in the case of soil chronosequences, the youngest soil profiles (Merritts et al., 1992; White et al., 1995). The assumptions inherent in this approach is that such materials are truly unweathered and that they accurately reflect the composition of initial sediments from which the older and more weathered soils were derived.

The second requirement in the mass balance approach (Eqns. 3 and 5) is that weatherable elements or minerals must be ratioed against an inert component i present in both the parent material and soil. Conservative elements most often employed in mass balance calculations include Zr (Harden, 1987; Chadwick et al., 1990), Ti (Johnsson et al., 1993), and rare earth elements such as Nb (Brimhall and Dietrick, 1987). Considerable disagreement occurs in the literature as to the relative mobility of specific elements under differing weathering regimes. Also as discussed by White et al. (1995), minor elements such Zr and Ti are often concentrated in the small size-heavy mineral fraction which may be subjected to significant fractionation during sediment transport and deposition.

An alterative approach is to consider relatively inert minerals such as ilmenite (April et al., 1986) and quartz (Sverdrup, 1990; White et al., 1995) as conservative phases. Quartz is often a significant fraction of the parent material and is of comparable particle size and specific gravity to the weatherable aluminosilicate fraction. Thus, quartz is less likely to fractionate in a depositional environment relative to heavy minerals containing elements such as Zr and Ti. However, the rate of quartz weathering in soil environments is open to debate and therefore the extent to which it is conservative relative to other weatherable minerals or elements is open to question. Based on experimental rate data, Lasaga et al. (1994) estimated that the residence time of 1 mm quartz grains at neutral pH to be 34 m yr, a time span 1 to 2 orders of magnitude longer than for feldspar grains of comparable size. White et al. (1995), demonstrated minimal etch pitting and relative constant BET surface areas for quartz in a 3 mA soil chronosequence. However other studies have suggested that significant amounts of quartz can dissolve in some weathering environments (Brantley et al., 1986; Brimhall and Dietrick, 1987) (see Dove, this volume; for a detailed discussion of quartz dissolution).

Use of mass balance equations

The preceding mass balance approaches are now illustrated for deep saprolitic weathering in the Rio Icacos watershed in Luquillo Mountains of Puerto Rico (White et al., 1995) This watershed is situated in a humid tropical rain forest. Bulk soil and bedrock samples were analyzed for major and minor elements. Soil density measurements were obtained using a piston coring device. The density of the granitic rocks was assumed to be $\rho_p = 2.60$. Resulting data, as functions of residual enrichment, ρ_p/ρ_w, strain $\epsilon_{j,w}$, and mass transport $\tau_{j,w}$, as defined in Equation (5), are plotted in Figure 1. In the Rio Icacos soil profile, the density ratio of parent rock to weathered saprolite ρ_p/ρ_w is larger in the shallow A soil horizon (<1 m) due to organic input and bioturbation (Fig. 1A). Deeper in the undisturbed sapolite B horizon, the profile reaches a relative constant density ratio of 2.0 (50% porosity) to a depth of approximately 7 m, which corresponds to the bedrock interface.

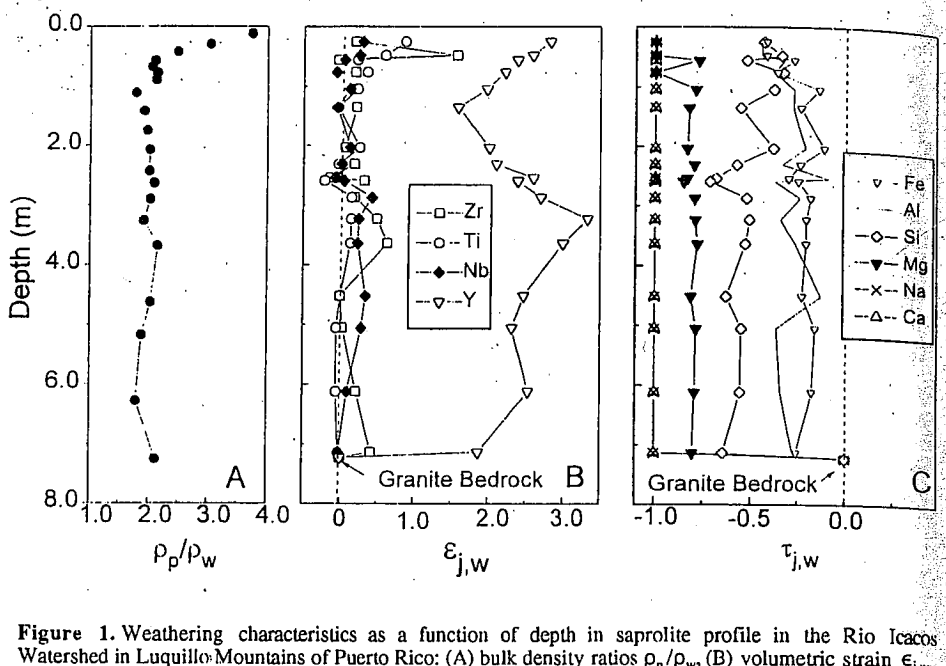

Figure 1. Weathering characteristics as a function of depth in saprolite profile in the Rio Icacos Watershed in Luquillo Mountains of Puerto Rico: (A) bulk density ratios ρ_p/ρ_w, (B) volumetric strain $\epsilon_{j,w}$, and (C) mass transfer $\tau_{j,w}$ calculated from Equations (5-7).

The calculation of the strain factor $\epsilon_{j,w}$,which describes the volume change in the soil ($\epsilon_{j,w} = V_w/V_p - 1$; Eqn. 7), was made using trace elements including Zr, Ti, and the rare earth elements Nb and Y (Fig. 1B). Although such elements are generally considered immobile with respect to weathering, their conservation under any specific geochemical condition is not guaranteed. Therefore, the best strategy is to consider a suite of such elements to establish the extent of volumetric changes undergone by a soil during weathering. As indicated for the Rio Icacos soil, Zr, Ti, and Nb produce consistent estimates for strain $\epsilon_{j,w}$ which center close to zero (Fig. 1B, vertical dashed line). This lack of a significant volume change indicates that weathering is essentially iso-volumetric, which is consistent with a soil porosity of nearly 50%, and with the preservation of primary igneous textures in the saprolite. Iso-volumetric weathering has been reported for other sapprolites based on mass balance calculations (Cleaves, 1993). Use of Y in Equation (7) produces calculated volume increases of up to a factor of three in the saprolite. Such unrealistic increases in volume reflect the loss of Y from the soil during weathering.

The mass transport component $\tau_{j,w}$ (Eqn. 6) is calculated for major cations and SiO_2 in the Luiquillo soil in Figure 1C. Values of -1 for Na and Ca throughout the profile indicate that these elements are completely loss during weathering of the primary silicates, principally from plagioclase and hornblende, and are not retained by secondary clay minerals, principally kaolinite. Approximately 80% of Mg, and 50% of SiO_2 are also lost. The only remaining primary minerals are hydrobiotite, which accounts for the residual Mg, and quartz, which along with secondary kaolinite, which accounts for the remaining SiO_2. Residual Al and Fe are retained in the kaolinite and Fe oxyhyroxide phases. The extent of elemental and mineral losses from weathering in the upper 7 m of the soil profile is constant. Current weathering occurs within a narrow interface (< 10 cm) directly above the underlying quartz diorite and overlying saprolite (Fig. 1).

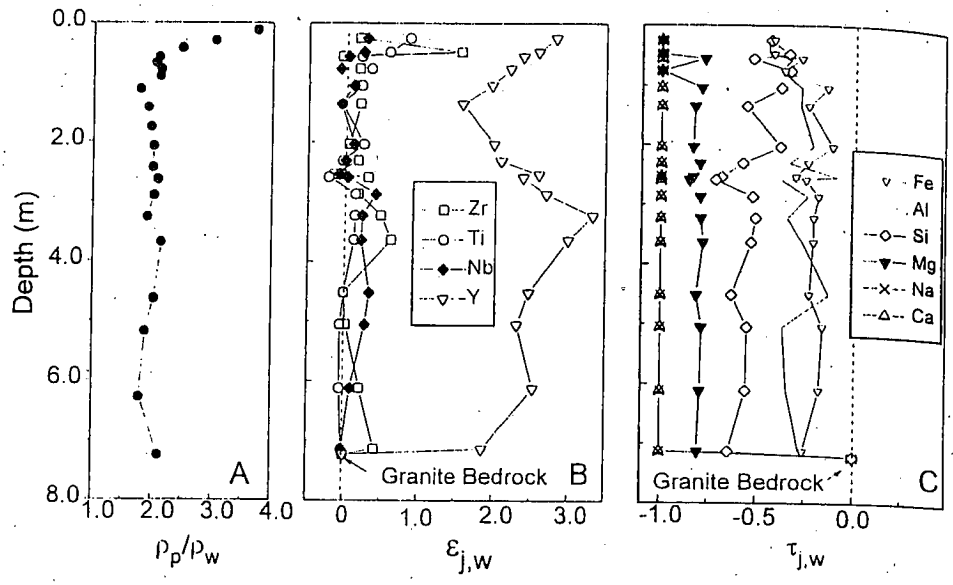

Figure 1. Weathering characteristics as a function of depth in saprolite profile in the Rio Icacos Watershed in Luquillo Mountains of Puerto Rico: (A) bulk density ratios ρ_p/ρ_w, (B) volumetric strain $\epsilon_{j,w}$, and (C) mass transfer $\tau_{j,w}$ calculated from Equations (5-7).

The calculation of the strain factor $\epsilon_{j,w}$, which describes the volume change in the soil ($\epsilon_{j,w} = V_w/V_p - 1$; Eqn. 7), was made using trace elements including Zr, Ti, and the rare earth elements Nb and Y (Fig. 1B). Although such elements are generally considered immobile with respect to weathering, their conservation under any specific geochemical condition is not guaranteed. Therefore, the best strategy is to consider a suite of such elements to establish the extent of volumetric changes undergone by a soil during weathering. As indicated for the Rio Icacos soil, Zr, Ti, and Nb produce consistent estimates for strain $\epsilon_{j,w}$ which center close to zero (Fig. 1B, vertical dashed line). This lack of a significant volume change indicates that weathering is essentially iso-volumetric, which is consistent with a soil porosity of nearly 50%, and with the preservation of primary igneous textures in the saprolite. Iso-volumetric weathering has been reported for other sapprolites based on mass balance calculations (Cleaves, 1993). Use of Y in Equation (7) produces calculated volume increases of up to a factor of three in the saprolite. Such unrealistic increases in volume reflect the loss of Y from the soil during weathering.

The mass transport component $\tau_{j,w}$ (Eqn. 6) is calculated for major cations and SiO_2 in the Luiquillo soil in Figure 1C. Values of -1 for Na and Ca throughout the profile indicate that these elements are completely loss during weathering of the primary silicates, principally from plagioclase and hornblende, and are not retained by secondary clay minerals, principally kaolinite. Approximately 80% of Mg, and 50% of SiO_2 are also lost. The only remaining primary minerals are hydrobiotite, which accounts for the residual Mg, and quartz, which along with secondary kaolinite, which accounts for the remaining SiO_2. Residual Al and Fe are retained in the kaolinite and Fe oxyhyroxide phases. The extent of elemental and mineral losses from weathering in the upper 7 m of the soil profile is constant. Current weathering occurs within a narrow interface (< 10 cm) directly above the underlying quartz diorite and overlying saprolite (Fig. 1).

The element loss from the Rio Icacos soil profile can be calculated by integrating $\tau_{j,w}$ over the depth of the entire profile z using Equation (9) and the composition and density of the bed rock (ρ_p = 2.60).The calculation indicates that for 1 m^2 of soil surface, the molar losses from weathering to a depth of 7 m are Si = $1.1 \cdot 10^5$, Ca = $1.7 \cdot 10^4$ Al = $1.6 \cdot 10^4$, Na = $1.1 \cdot 10^4$, Mg = 6.4×10^3, Fe = $2.3 \cdot 10^3$ and K = $2.0 \cdot 10^1$. Elemental fluxes, when combined with known stoichiometries, can be used to calculated the total mineral mass flux M_j (Eqn. 1).

Elemental losses as functions of time

If the age of a soil horizon is known, mass loss as function of time can be determined from Equations (3) or (5). The most direct application of this approach is to soil chronosequences. The following example demonstrates the usefulness of this approach in interpreting effects of climate on chemical weathering rates for 3 soil chronosequences studied in California. These soils are described briefly as follows:

The *Merced Chronosequence* is comprised of soils developed on alluvial terraces formed from glacially-derived granitic outwash from the Sierra Nevada and deposited along the Merced River in central California (Harden, 1987). The main soil units and estimated ages of these deposits (0.2 to 3000 kA) obtained by ^{14}C, uranium trend analysis, and K-Ar dating methods are listed in Table 2. The present climate is a Mediterranean type with average annual precipitation of 300 mm and an average temperature of 16 °C.

The *Honcut Creek Chronosequence* is a series of soils developed on alluvial outwash terraces from the Sierra Nevada and consisting of meta-volcanics and granodiorite were developed along to the north near the Feather River Canyon. These soils, described in detail by Busacca and Singer (1989), range in age from 0.6 to 1600 kA. The present climate is Mediterranean with an average annual rain fall of 600 mm and an average annual air temperature of 16 °C.

The *Strawberry Rock Chronosequence* is situated near the mouth of the Mattole River in Northern California and is composed of marine terrace deposits composed of arkosic sandstone with some siltstone and shale from the Jurassic Franciscan formation. Soil ages are based on radiocarbon and sea-level stands, and range from 3.6 to 240 kA (Chadwick et al., 1990; Merritts et al., 1992). This site has a seasonal Mediterranean type climate characterized by prolonged cool but dry summers and mild and wet winters with an annual precipitation of 1100 mm and an average annual temperature of 13°C.

The ratios of SiO_2 concentrations in the soil and parent sediments (R_o, Eqn. 3) were chosen as indicators of the extent of weathering within the soil chronosequences. In both the Strawberry Rock and Honcut Creek studies, Zr was assumed to be the conservative component (Busacca and Singer, 1989; Merritts et al., 1992) while quartz was assumed to be chemically conservative in the Merced soils (White et al., 1995). All three studies assumed that the deepest C horizons of the youngest soils were representative of parent chemical compositions. The SiO_2 ratios for the Merced, Honcut Creek and Strawberry Rock soils are approximated by exponential decay functions when plotted against time in Figure 2A (solid lines). Such exponential decay functions have been observed for other chemical properties of chronosequences such as the decrease in base cation saturation with time (Bain et al., 1993). These exponential decreases in weathering rates are attributable to selective removal of the more reactive minerals during the initial stages of weathering and the persistence of less reactive phases during later stages of weathering.

The relative rates of SiO_2 decrease in the three soil chronosequences are significantly different. The Strawberry Rock soils weather faster than the Honcut Creek soils which in turn weather faster than the Merced soils (Fig. 2A). These relative rates are apparently related

Table 2. Soil profiles and ages of the Merced Chronsequence, California.

Soil Unit	Sampled Depth (cm)	Age of surface (kA)
Post-Modesto Deposits	51	0.2 - 3
Modesto Fm., Upper member	254	10
Modesto Fm., Lower member	413	40
Riverbank Fm., Upper unit	400	130
Riverbank Fm., Lower unit	500	250
Turlock Lake Formation	375	600
Laguna Fm., China Hat Unit	350	3000

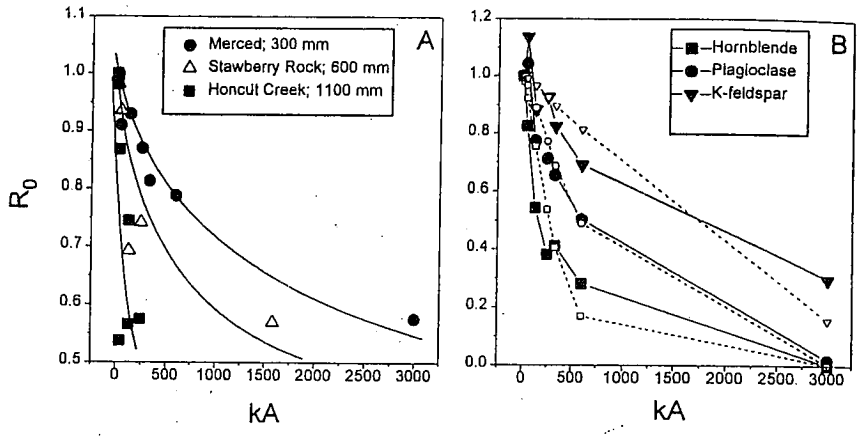

Figure 2. Comparison of mineral weathering rates based on mass ratios (R_o) for: (A) decrease in SiO_2 as a function of time for three chronosequences in California legend (annual precipitation in mm), and (B) decrease in mineral abundances with time for the A horizons in the Merced chronosequence. Dashed lines connect fitted rate constants k_j (Eqns. 21 and 22).

to climatic differences. Although the current mean annual air temperatures for the 3 chronosequences are similar, 14-16 °C, the average annual precipitation varies by almost a factor of 4 from 300 mm for the Merced soils to 1100 mm for the Strawberry Rock soils. A comparable correlation between increasing weathering and precipitation has been recently documented for SiO_2 and Na in watershed studies (White and Blum, 1995b). Comparison of weathering rates of soil profiles based on present climate assumes that similar conditions have persisted in the past. Precipitation in central California reached a long term maximum in the late Pliocene at approximately 1.5 times that of the present day average (Busacca et al., 1989). Past paleoclimatic differences at an individual site therefore appear to be less than present day differences between the 3 sites. Other mass balance studies have investigated differences in weathering rates over time. Cleaves (1993) estimated that the rates of saprolite formation in the Piedmont Province in Maryland may have decreased by 50 to 90% as a result of periglacial conditions during the Pleistocene.

Mineral losses as functions of time

The mass balance calculations use ratios for both weatherable and inert components

Table 3. Comparsion of compositions of parent Tuolume intrusive series and basal C horizons of the 10 kA Merced soils. Units are in wt % unless otherwise indicated.

Unit	Profile[2]	Depth	Qtz.	Plag.	K-feld	Hnbl.	Biot.	Clay	Zr	Ti
Granite[1]			25.4	43.9	22.2	7.0	4.1	0.0	0.016	0.37
Basal Modesto	M12	231 cm	34.6	38.7	15.7	7.0	3.2	0.8	0.017	0.36
Basal Modesto	M31	254 cm	37.2	33.0	12.9	10.7	2.6	3.6	0.033	0.57
Basal Modesto	M46	250 cm	33.6	39.4	10.8	5.7	1.8	8.7	0.021	0.49

[1]Data from Bateman and Chappell, 1989; [2]Units based on classification of Harden, 1987

(Eqns. 3 and 5) and are therefore equally applicable for calculating mineral as well as elemental losses or gains (White et al., 1995). Mineralogical compositions in soils and parent material can be determined using a number of analytical approaches including point counting, chemical modal analysis and quantitative X-ray diffraction techniques. The last two techniques were used to evaluate mineralogical changes in the Merced chronosequence soils (White et al., 1995). As indicated in Table 3, the composition of the assumed parent materials, as represented by the basal C horizons of the youngest 10 kA soils, are significantly depleted in feldspars and enriched in quartz relative to the source granite contained in the Tuolumne intrusive of the Sierra Nevada. Note also that quartz abundances are much more consistent within the deposits than are Zr and Ti contents which are commonly assumed to be conservative elements in mass balance calculations (Eqns. 3 and 5) These differences are attributed to weathering and preferential sorting of heavy minerals prior to deposition in river terrace deposits.

The proportions of K-feldspar, plagioclase and hornblende remaining in the A soil horizons relative to the parent composition were calculated and plotted as a function of soil age in Figure 2B. R_n values, based on quartz as the conservative component, approach unity in the younger soils (±0.20). During the first 600 kyr, primary silicates decrease exponentially in order hornblende > plagioclase > K-feldspar, which is consistent with commonly observed weathering rates in soils (Dixon and Weed, 1989; Nahon, 1991) and in experimental dissolution studies (Lasaga, 1984). The calculations predict, that after 3000 kyr, all of the primary aluminosilicate minerals are lost except for a residual K-feldspar fraction (R_n = 0.30). Optical inspection of residual mineral separates in the China Hat showed no detectable plagioclase or hornblende and only minor amounts of K-feldspar. Decreases in reactive minerals dominate the initial weathering processes and result in rapid SiO_2 loss in younger soils. In the older soils, chemically resistant minerals, principally quartz, are present. The selective decrease in reactive minerals explains the exponential decrease in chemical weathering rates with time.

Other studies have also used changes in mineral abundances to investigate chemical weathering. Mahaney and Halvorson (1986) documented progressive increases in the quartz/feldspar ratios in soils from a 500 kA chronosequence in the Wind River Mountains of Wyoming. April et al. (1986) calculated long term chemical weathering rates based on hornblende depletion in soils in two Adirondack watersheds. In comparing these rates with weathering based on watershed solute discharge, these workers concluded that current rates may be a factor of 3 times greater than long term rates due to the influence of acid deposition. As in the case of elemental loses (Fig. 2A) mineral losses can provide important information on changes in the weathering environment over time (Fig. 2B).

Volumetric analysis and rates of soil formation

Chemical weathering rates in soils can, in some instances, be formulated as the rate of downward movement (velocity) of the chemical weathering front into the regolith. The simplest case is the use mass balances to investigate the iso-volumetric weathering of crystalline bedrock to saprolite (Cleaves, 1993). As indicated for the Rio Icacos soils, weathering of primary minerals occurs predominantly at the base of the saprolite in direct contact with the bedrock (Fig. 1). Mass balance under such conditions requires that the volume of saprolite equals the volume of initial rock ($V_w = V_p$). A unit volume of saprolite v_{sp} therefore can be considered to consist of three components: the volume fraction of secondary minerals produced from weathering v_{sm} (e.g. clay and Fe oxyhydroxides), the volume fraction of stable unweatherable minerals v_i (e.g. quartz) and the volume fraction due to porosity of the saprolite v_p such that

$$v_{sp} = v_{sm} + v_i + v_p \tag{10}$$

The velocity of the weathering front at the saprolite-bedrock interface ω_{sp} (cm s^{-1}) can be related to the mass flux of solute transported from the weathering profile Q_w (g cm^2 s^{-1}) where ρ_p is the density of parent rock (g cm^3)

$$\omega_{sp} = \frac{Q_w}{\rho_p} \cdot \frac{1}{v_{sm}} \tag{11}$$

Q_w is most often determined from net watershed mass fluxes attributed to chemical weathering in the soil profile. Methods for calculating weathering rates in watersheds based on mass balances are discussed in detail by Drever (this volume). Weathering fluxes are determined as the difference between total measured solute discharge in the stream and input and output sources such as wet and dry fall, biological fluxes and ion exchange. Solute fluxes attributed to weathering can be normalized to the geographical surface area of the watershed which in turn can be converted to unit area of soil (g. cm^{-2}).

Cleaves (1993) calculated a range of weathering velocities of ω_{sp} = 3.7 to 29.7 m 10^{-6} yrs for the vertical advancement of the saprolite weathering front into schists in the Pond Branch watershed in the northern Piedmont Province of the USA. Other saprolite weathering rates, including that for granite at the Rio Icacos site, are found to range between 3 and 37 m 10^{-6} yrs (Table 4). Such rates are also comparable to long term denudation rates reported for comparable landscapes assuming long term dynamic equilibrium between rates of saprolitization and rates of physical and chemical erosion. Based on total river discharge, sediment rates and solute fluxes (Wakatsuki and Rasyidin, 1992) estimated a global average soil formation rate of 5.6 m 10^{-6} yrs.

In contrast to iso-volumetric weathering of bedrock to saprolite, soil formation on sedimentary deposits commonly results in significant increases in soil density and decreases in soil volume with time. For example, measured bulk densities ρ_w of the Merced chronosequence (Fig. 3A) increase with age from the Post Modesto (3 kA) through the Turlock Lake (600 kA) soils and then decrease in the China Hat (3000 kA) soils. Density increases in the older soils are related to soil compaction associated with weathering of primary minerals and clay formation. Less compaction in the oldest China Hat soil is probably due to the presence of cobbles which support a less dense soil structure. Higher organic contents and bioturbation create lower bulk densities in the A horizons than the B+C horizons.

Corresponding volume changes for the B+C horizons of Merced soils based on

Table 4. Propagation rates of weathering fronts at the sapolite/bedrock interface (Eqn. 11). Weathering rates are in meters/10^6 years.

Rate	Rock		Reference
3.3-29.7	Schist	Pond Branch Maryland	Cleaves, 1993
4.0	Granite	Occoquan basin, Virgina	Pavich et al., 1986
35.8	Granite	Rio Icacos, Puerto Rico	This paper
37.0	Schist	Coweeta Watershed, North Carolina	Velbel, 1985

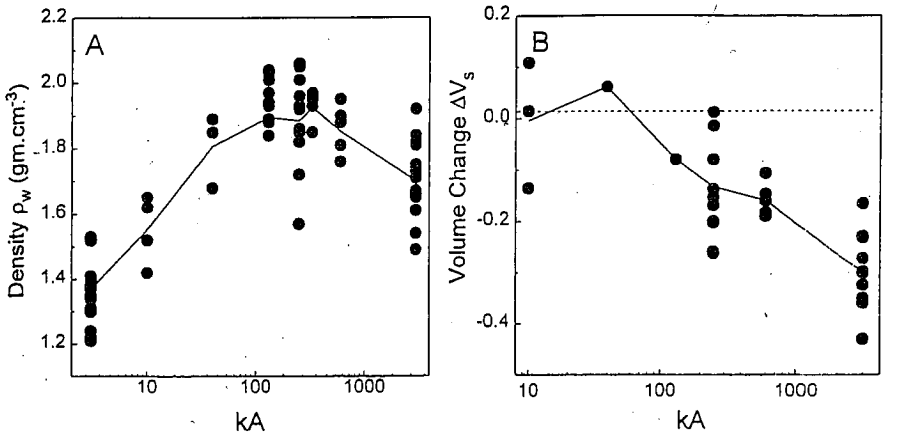

Figure 3. Density ρ_w and volume change ΔV in the B+C horizons of soils in the Merced chronosequence. Lines connect mean average values of soil samples of the same age.

Equation (4) are plotted as functions of time in Figure 3B. The progressive decrease in the volume ratio to 0.7 in the oldest China Hat soils suggest that significant compaction has occurred as a result of weathering even though the bulk densities in the younger soils actually increase (Fig. 3A). Assuming that (1) quartz is conservative, (2) parent mineralogy is equivalent to the average composition listed in Table 3 and (3) ρ is constant for all minerals, the complete weathering of aluminosilicates to kaolinite would produce a volume loss of 30%, which is comparable to the calculated China Hat volume loss (Fig. 3B). The extent of these volumes losses are expected to significantly affect porosity and hydrochemical processes which control weathering in the soils.

The approaches presented in the preceding discussions are important techniques in quantifying mass and volume losses associated with the weathering of primary minerals in soils. When normalized relative to spatial distributions, such mass balances provide information on total mass losses from soil horizons (Eqns. 8 and 9). When coupled with soil ages, mass balances permit comparison of relative weathering rates in different soil profiles and to assess parameters such as climate differences.

SOIL SURFACE AREAS

The calculation of quantitative dissolution rates k_j (Eqn. 1) is dependent on normalizing the reacted mineral mass M_j to the mineral surface area S. As will become apparent in the following discussion, the estimation of surface areas is one of the most difficult problems in quantifying weathering rates in soils and represents one of the sources of greatest discrepancy. The surface area in Equation (1) is related to the density of sites on

the solid surface which is exposed to aqueous solution and at which silicate hydrolysis reactions can occur (Helgeson et al., 1984). However, from an operational standpoint, such reactive surface areas in natural weathering studies are almost always assumed to scale directly with measurable physical surface areas ($cm^2\ g^{-1}$). The following discussion will therefore focus principally on available data and methods for determining physical surface areas of primary minerals in soils. Other factors, including selective reaction at defect and dislocation sites and physical and hydrologic isolation of mineral surfaces, may decouple physical and reactive surface areas. Additional discussions of the nature of reactive surfaces are presented in a following section of this present paper and elsewhere in this volume (see Lasaga; Blum and Stillings).

Assuming spherical grain geometry for a non-porous mineral, the specific surface area S ($cm^2\ g^{-1}$) of mineral grains of constant diameter D (cm) can be described as (Jaycock and Parfitt, 1981; Anbeek, 1992)

$$S = \frac{6}{\rho_j D} \lambda \tag{12}$$

where ρ_j ($g\ cm^{-3}$) is the mineral density and λ ($cm^3.cm^{-3}$) is the roughness factor. λ is the ratio of the measured surface area S to the equivalent geometric surface area s (Helgeson et al., 1984; White and Peterson, 1990; Anbeek, 1992) such that

$$\lambda = S/s \tag{13}$$

Operationally surface roughness is determined from a macroscopic measuring technique used to estimate s (e.g., sieving or light scattering) and a microscopic technique used to measure S (e.g. BET gas sorption). S can be defined by Equation (13) as the product of the spherical geometric surface area s ($cm^2\ g^{-1}$), defined by D and ρ_j, and the roughness factor λ (cm^3/cm^3).

Surface areas of silicate minerals in soils

Surface areas of soil components are commonly normalized to soil mass ($m^2\ gm^{-1}$ of soil) or as a specific surface area normalized to the unit mass of mineral component ($m^2\ g^{-1}$ of mineral). BET surface areas of bulk soils are generally reported to range between 5-70 m^2 per gram of soil (Gallez et al., 1976; Feller et al., 1992). Limited data on the surface area of the primary silicate fraction suggests that this component makes up a minor portion of the bulk surface area. White and Peterson (1990) investigated the relationship between grain size distributions and surface areas of the silt-sand size fractions of several soils. Examples included the relative contributions of Fe-oxyhyroxides, Fe-silicate phases (≈ biotite + hornblende) and non-Fe containing silicates (feldspars + qtz) to total surface areas of a poorly developed soil on Sierra Nevada granite near Lake Tahoe (Fig. 4A) and a deeply weathered granitic saprolite from Montara Mountain near San Francisco (Fig. 4B). Data are plotted as cumulative contributions to the bulk surface area (m^2 per gram of soil) In the younger soil, the surface area of all size fractions are dominated by Fe-oxyhyroxide phases which coat the silicate grains. This contribution is less in the older Montara soil with surface area being dominated by the residual primary Fe-silicate phases. In both soils, the combined surface areas of quartz and feldspar in all size fractions were only a minor component of the total soil surface area.

Soil surface areas generally increase with soil age (Table 5). The BET surface areas of Merced soils increase with age from 4 to 18 m^2/g. This increase correlates closely with the corresponding clay content whose surface areas comprise about 20% of the total surface area in the youngest 3 kA soils, compared to 72% in the oldest 3000 kA soils. Cumulative surface

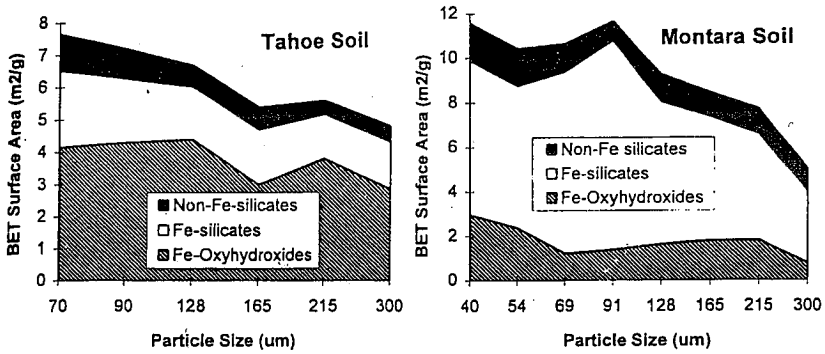

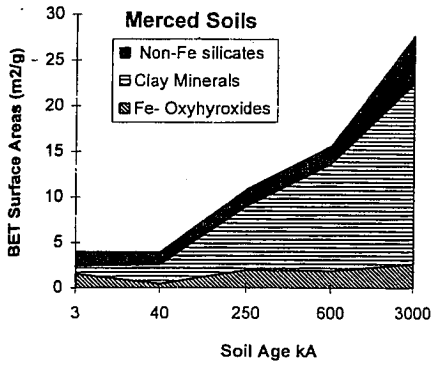

Figure 4 (above). Cumulative BET surface areas (per gm of soil) versus grain size for Montara and Tahoe soils.

Figure 5 (left). Cumulative BET surface areas (per gm of soil) versus age of soil profiles in the Merced chronosequence.

Table 5. BET surface areas of soil and mineral components of the Merced chronosequence ($m^2\ g^{-1}$)

Unit	Post Modesto	Modesto	Riverbank	Turlock Lake	China Hat
Age (kA)	3	40	250	600	3000
Profile	PM14	M12	R32	T6	CH2
Depth (cm)	33-99	32-66	152	100-155	90-130
Soil Horizon	C	A	B	B	B
Surface Areas of Soil Components					
Untreated Soil	4.47	4.11	7.51	10.25	17.68
Extractable Fe	1.58	0.49	2.00	1.91	2.67
Clay (<4 um)	0.87	2.10	7.00	11.74	19.80
Silicates (>4 um)	1.52	1.32	1.81	1.92	5.18
Surface Areas of Mineral Separates[1,2]					
Quartz	0.11	0.17	0.23	0.21	0.10
Plagioclase	0.39	0.26	0.46	1.48	na
K-feldspar	0.12	0.26	0.94	0.81	na
Hornblende	na	0.34	0.72	0.67	na

[1]Fe removed by dithionite

[2]Analysis for 500 to 1000 um fraction except hornblende (500-250 um)

areas contributed by primary silicates, clay, and Fe-oxyhydroxides, per gram of soil, are plotted as functions of age in Figure 5 (White et al., 1995). Due to increasing clay content and decreasing abundance, the contribution of primary silicate fraction to the bulk soil surface area decreases from 37% in the youngest soils to 18% in the oldest soils. The preceding data indicate that although the surface areas of the primary silicate fractions are critical in controlling weathering rates, their relative contribution to bulk soil surface area is generally minor.

Very limited information is available on the specific surface area of primary mineral phases in soils. White et al. (1995) documented that the specific surface area of plagioclase grains increases with age from 0.4 $m^2 g^{-1}$ in the 3 kA Post-Modesto to 1.5 $m^2 g^{-1}$ in the 600 kA Turlock Lake soils (Table 5). K-feldspar and hornblende exhibit more erratic but significant increases in surface area over the same period (Fig. 6A). In the oldest China Hat soil only residual quartz was abundant enough for BET measurements. This quartz surface area was comparable to quartz in the younger soils (0.1-0.2 $m^2 g^{-1}$) suggesting significant resistance to chemical weathering in this environment.

Surface area and particle size

Equation (12) predicts that the external surface area is proportional to the geometric surface area. Therefore a plot of *log S* versus *log D* should produce an inverse relationship with a slope of -1 as documented (White and Peterson, 1990) for clays, oxides and freshly crushed silicates (Fig. 7). The parallel offset in the data relative to the geometric surface area *s* is equal to the average surface roughness ($\lambda = 7$) which was independent of particle size. In reviewing surface area for crushed quartz and natural well-rounded quartz grains, Parks (1990) also found surface roughnesses ($\lambda = 2.2$ and 6.2, respectively) that were independent of grain size. In reviewing BET surface area data for crushed feldspar samples employed in dissolution studies Blum (1994) determined a corresponding roughness factors of 9±6. BET surface areas of relatively unweathered minerals are therefore generally proportional to their particle diameter based on an assumed spherical geometry. Likewise the deviation in the magnitude of measured and geometric surface areas over large ranges in particle diameter are relatively constant ($\lambda = 2$ to10).

Surface Areas of Weathered Silicates

BET surface areas of the primary silicate fraction weathered in soils is significantly larger than for the corresponding freshly crushed and unweathered minerals. White and Peterson (1990) reported surface roughnesses of $\lambda = 50$ to 200 for the sand size primary silicate fractions of several soils development on granitic bedrock. Anbeek (1992) reported roughness factors of $\lambda = 130$ to 2600 for silicates from glacial deposits in Switzerland. BET surface area data versus silicate particle size (feldspar + quartz) from 5 soils from the Merced chronosequence are plotted in Figure 8. Aggregated clay particles and Fe-oxyhyroxide coating were removed by pre-treatment. For any size fraction, the BET surface areas of the silicate minerals are much larger ($\lambda = 100$ to 1000) than the corresponding spherical geometric surface area (dashed line, Fig. 8). The weathered surface areas are also significantly larger ($\lambda = 10$ to 100) than BET surface areas of similar size fractions of freshly crushed silicates commonly used in experimental dissolution studies. The surface areas of particles of the same diameter in the Merced soils also generally increase with soil age.

The surface areas for weathered grains have a log slope less than -1 and are clearly non-linear relative to particle size (Fig. 8). The difference between the measured BET surface area and the equivalent geometric surface area decreases with decreasing grain size indicating that the apparent surface roughness also decreases with size. Anbeek et al. (1994)

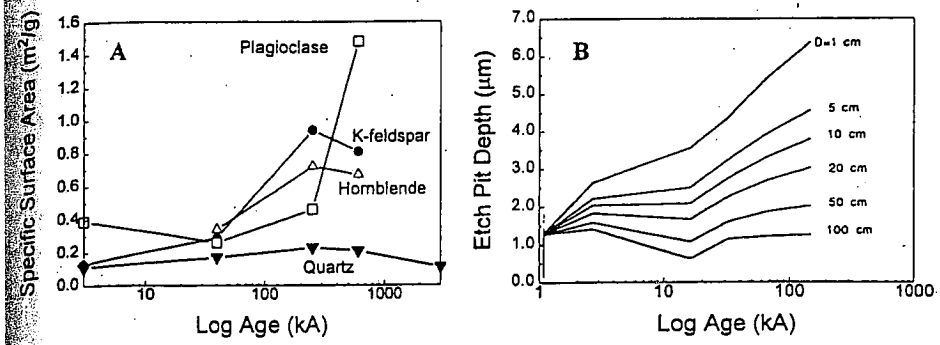

Figure 6. Specific BET surface areas of minerals in Merced chronosequence (A) and etch pit depth of hornblende in the Tobacco Range chronosequences (B) (Hall and Horn, 1995) as functions of soil age. D corresponds to soil depth.

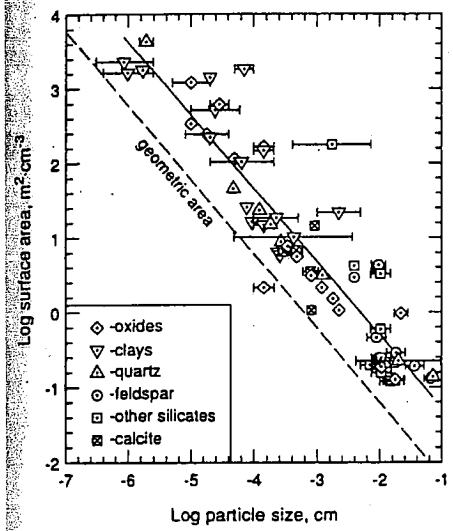

Figure 7. Relationship between reported BET surface areas and grain size for non-weathered minerals (White and Peterson, 1990). Dashed line corresponds to the geometric surface area and solid line to the linear regression fit through the BET data (slope = -0.99, r^2 = 0.86).

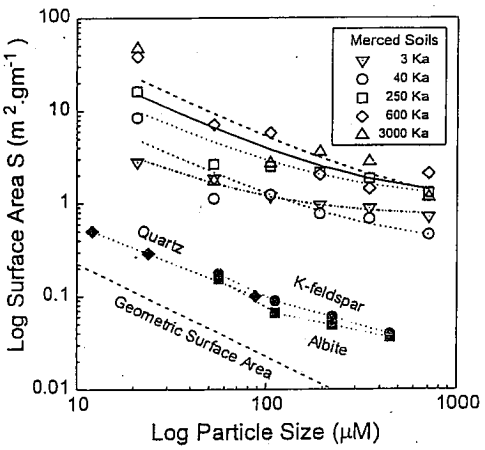

Figure 8. Surface area as a function of particle diameter (from White et al., 1995). Geometric areas are calculated for smooth spheres of equivalent diameter (dashed line). Quartz, K-feldspar and albite data are BET measurements of freshly crushed material (Leamnson et al., 1969; Holdren and Speyer, 1987). Curved lines are fits of Equation (16) to the BET measurements of silicate fractions (less clay and Fe oxyhydroxides) of Merced soils of different ages (open symbols).

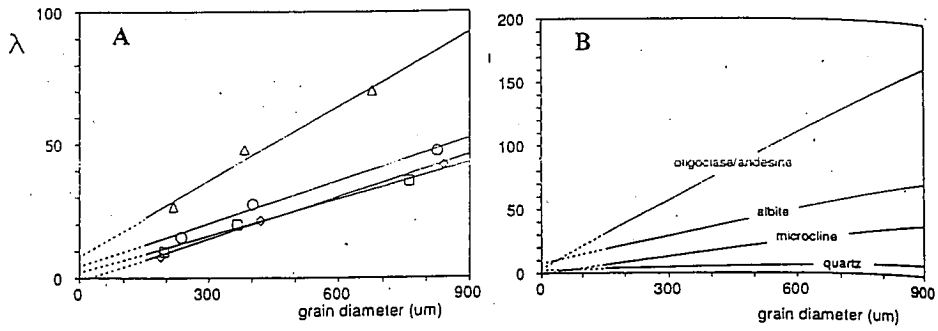

Figure 9. Relationship between surface roughness λ and grain diameter for the bulk silicate fraction (A) and individual minerals (B) from glacial deposits from Switzerland (from Anbeek et al., 1994).

also investigated the relationship between surface roughness and particle sizes for weathered silicates from glacial deposits. As shown in Figure 9 surface roughness for both the bulk samples and individual mineral fractions decrease linearly with particle diameter. Decreases in surface roughness for naturally weathered silicates contrasts with the apparent constant roughness factors for unweathered silicates and oxides as summarized by Parks (1990) and White and Peterson (1990) (Fig. 7).

Surface roughness of weathered silicate grains in soils is related to microscopic morphologic features on grain surfaces not considered in geometric estimates. Pervasive etching and pitting during weathering of primary minerals in soils have been previously observed for pyroxenes and amphiboles (Berner et al., 1980; Velbel, 1989; Cremeens, 1992) feldspars (Berner and Holdren, 1979; Cremeens, 1992; Brantley et al., 1993) and quartz (Brantley et al., 1993). These studies conclude that roughening is due principally to etch pit formation resulting from preferential dissolution from reactive sites with high surface energies at dislocation, defect sites and exsolution lamellae. Several models have been proposed to quantitatively relate surface energies of such sites to the density and morphology of etch pits and dissolution rates (Lasaga; Blum and Stillings; Brantley; this volume).

Grain roughness and pitting have generally been found to increase with soil age. For example, SEM photographs of plagioclase surfaces from the Merced soils (Fig. 10) clearly show more extensive pitting in the 250 kA Riverbank soil relative to the 10 kA Modesto soil. However some grains of the same age and mineralogy were found have nearly pristine surfaces while others were highly weathered. Anisotropic dissolution of different crystallographic faces is commonly observed, and may explain a portion of this variation. This is seen in the 10 k A plagioclase from the Modesto Formation (Fig. 10A) in which the left facing surfaces are much more deeply pitted, and the 250 kA K-feldspar grain (Fig. 10C) in which the (001) cleavage faces (horizontal in the micrograph) are less pitted than surfaces with other orientations. However, heterogeneity is also observed on faces with a nearly constant orientation. This may reflect variations in the composition and/or defect structures of the mineral grains, or large variations in the chemical conditions of weathering micro-environments within the soil.

Efforts have been made to develop quantitative relationships between the extent and morphology of pitting and soil weathering environments using scanning electron and petrographic microscope techniques (Hall and Martin, 1986; Locke, 1986; Cremeens et al., 1992; Hall and Horn, 1993). An example of the relationship between etch pit depth and age of hornblende grains contained in a soil chronosequence developed on glacial moraines in

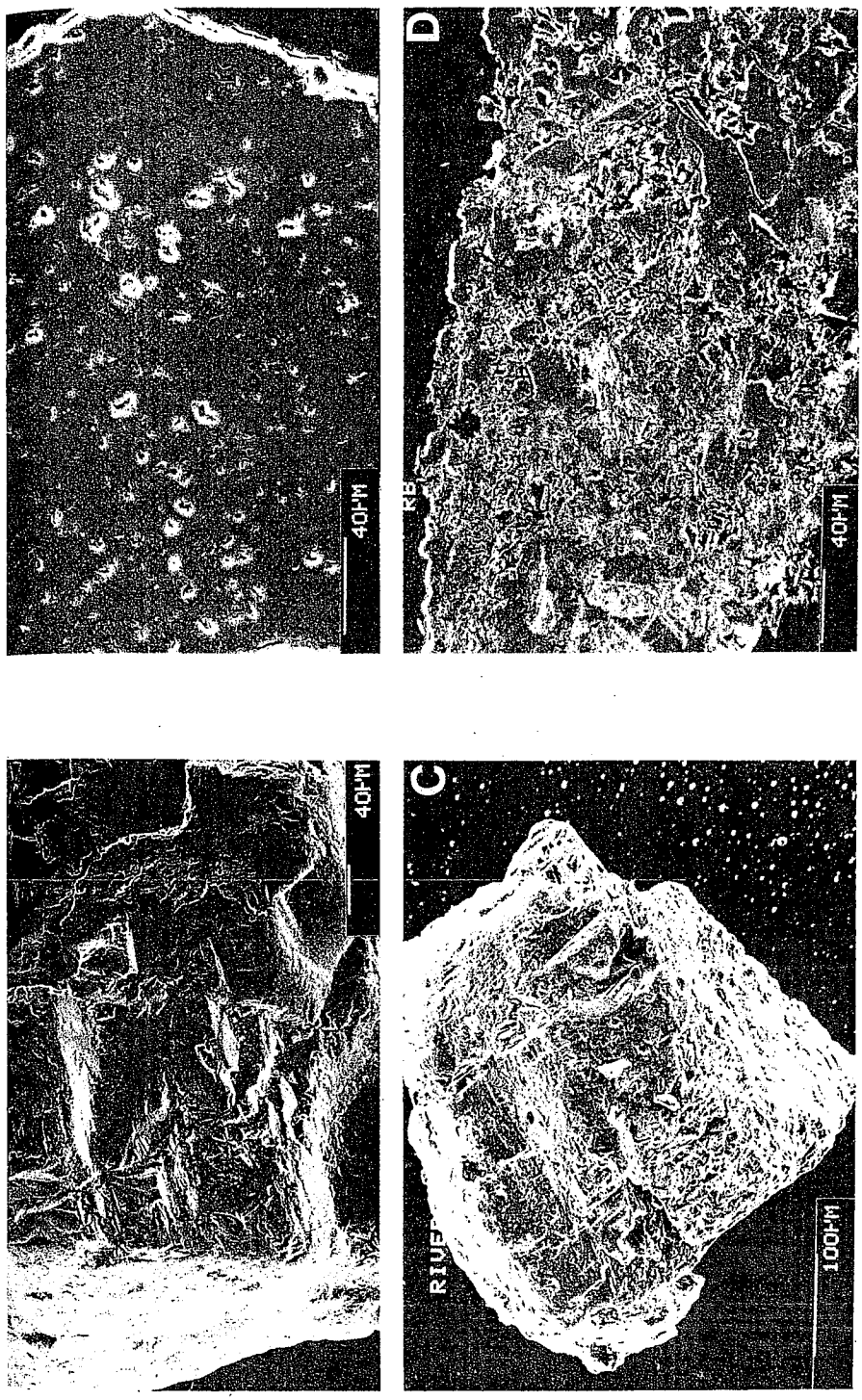

Figure 10. SEM photos of selective plagioclase grains in B horizons of the Merced soils. (A) and (B) are surface and thin section of a grain from the 10 kA Modesto soil. (C) and (D) are surface and thin section of a grain from a 250 kA Riverbank soil.

the Tobacco Root Mountain Range of Montana is shown in Figure 6B (Hall and Martin, 1986). The parent rock types are Precambrian metamorphic rocks and Cretaceous granites. As indicated, the depth of surface pitting of hornblende both increases with soil depth and age. This increase in etch pitting for minerals in the Tobacco Root chronosequence can be qualitatively compared to the increase in surface areas of the primary silicate fraction in the Merced chronosequence for comparable soil ages. This comparison suggests the importance of surface morphology in controlling BET surface areas. However a quantitative relationship between the degree of surface pitting and the surface roughness is not necessarily clear. For example, Anbeek et al. (1994) concluded that surface roughness attributed to etch pits on naturally weathered feldspar surfaces contributed only a fraction of the total measured surface areas.

Internal porosity

Several studies (Wood et al., 1990; Anbeek et al., 1994; and White et al., 1995) have concluded that weathered silicate minerals exhibit significant internal porosity which may be a major contributor to total mineral surface areas. SEM photomicrographs of cross-sectioned mineral grains show internal porosity, even in the youngest soils. However, as shown for examples of plagioclase from the Merced soils, the internal porosity is greater in the 250 kA Riverbank soil relative to the 10 kA Modesto soil. Morphologies range from small isolated equal-dimensional pits (Fig. 10B) to elongated and interconnected pores and cracks (Fig. 10 D). In general, pore diameters increase with soil age even though the absolute number of pores does not change appreciably. In the more highly-weathered grains, the pores enlarge and coalesce, finally forming very open internal structures (Fig. 10D). Pores are generally equally distributed from the rim to the core of grains, and do not form any weathering rim. In general the density of macropores increased in the order hornblende > plagioclase > K-feldspar > quartz which is in general agreement with the weatherability of silicate minerals (Goldich, 1938) and roughness factors calculated by Anbeek et al. (1994).

The distribution of macropores appears to be related to the internal distribution of defects. The density of internal pores counted in a typical cross-section photo of a weathered plagioclase from the Riverbank soil (250 kA) was found to be 500 pores per 5000 μm^2, which is a density of 10^7 cm^2 (White et al., 1995). This pore density is in the range of dislocation densities observed in feldspars from undeformed igneous rocks (Willaime et al., 1979). A surprising amount of porosity generated by these defects may be present within mineral grains before the onset of any soil weathering process. Porosities of up to 4% observed in unweathered plagioclase and K-feldspar have been attributed to exsolution of magmatic water and hydrothermal alternation within plutons (Montgomery and Brace, 1975; Worden et al., 1990). SEM photos produced by these studies show both tubular and equivalent micro-cavities that closely resemble pores permeating the weathered Merced feldspars (Fig. 10).

Calculation of combined surface roughness and internal porosity

For porous media with internal porosity accessible to the mineral surface, the total measured surface area S can be refined from Equation (12) (White et al., 1995),

$$S = \frac{6}{\rho D}\lambda + S_i \qquad (14)$$

where S_i (m^2/g) is the portion of the surface area associated internal porosity that is physically connected to the surface.

Table 6. External roughness λ and internal surface area S_i (m^2/g) for the primary silicate fraction of the Merced soils[1]

Soil Age	λ	λ*	S_i	S_i*
3	21	11	0.69	1.32
40	42	36	0.32	0.51
250	83	90	1.05	1.78
600	200	310	0.74	1.32
3000	130	620	0.99	5.81

[1] λ* and S_i* are calculated parameters excluding the quartz fraction (Eqn.15).

The total surface area S of very small particles will be dominated by the external surface area which is high relative to the total particle mass. Equation (14) then becomes equivalent to Equation (12) ($S = 6\lambda/\rho D$) and the slope approaches log S/log D = -1 for constant λ and ρ (Fig. 7). The total surface areas of very large particles will depend principally on the internal surface area ($S \approx S_i$) which is attributed to the porosity evident in SEM micrographs (Fig. 10). If porosity is evenly distributed throughout the grains, S_i will be independent of grain size and the slope approaches log S/log D = 0. For intermediate size particles, a dependence on both external and internal surface areas will predict a non-linear decrease in S with increasing D. Such a condition is evident for the relationship between primary mineral surface areas and particle diameters for the Merced soils which produces non-linear slopes between -1 and 0 (Fig. 8).

External roughness λ and internal surface area S_i can be determined by empirically fitting Equation (14) to observed surface area -grain size distributions such as plotted in Figure 8 (White et al., 1995). As shown in Table 6, roughness factors λ for the Merced soils were found to increase consistently with age from λ = 21 in the 3 kA Post Modesto soil to λ = 200 in the 600 kA Turlock Lake soil. The higher proportion of quartz in the China Hat soil explains the corresponding decrease in apparent surface roughness (λ = 130). Quartz BET surface areas are significantly lower than for other minerals and exhibit essentially no increase with soil age (Table 5).

Changes in surface roughnesses of the aluminosilicate fraction λ* (plagioclase + K-feldspar + hornblende + biotite) were estimated by correcting for dilution by quartz λ_{qtz} (White et al., 1995)

$$\lambda^* = \frac{\lambda - \lambda_{qtz} x_{qtz,w}}{x_{j,w}} \qquad (15)$$

$x_{qtz,w}$ and $x_{j,w}$ are the mass fractions of quartz and aluminosilicates in the soil. Resulting values for λ* show a consistent increase in surface roughness with soil age from λ = 11 for the 3 kA Post Modesto soil to λ = 620 for the China Hat soil (Table 6) Surface roughnesses λ* of the youngest Merced soils approach values of λ = 5 to 10 reported for freshly crushed silicates (White and Peterson, 1990; Blum, 1994). As shown in Figure (11), the divergence between λ* (open circles) and λ (closed circles) becomes more pronounced for the older soils as x_{qtz} increases. Surface roughness λ*of the residual aluminosilicate fraction in the oldest China Hat soils exceeds the range reported previously for weathered feldspar and granitic surfaces (White and Peterson, 1990; Anbeek, 1992) (λ = 50 to 500). The fitted roughness factors are assumed to be independent of grain size and can therefore be compared to roughness factors determined independently for individual minerals (Fig. 6A). As predicted, both λ and λ* are bracketed by λ values for plagioclase and quartz which exhibit respectively the largest and smallest increases in surface roughness with time.

Unlike external surface areas, internal surface areas reflecting grain porosity exhibit

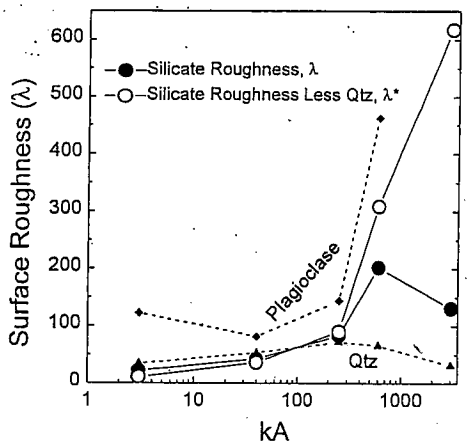

Figure 11. Calculated surface roughness as functions of soil age based on measured BET surface areas and calculations using Equations (14) and (15) (from White et al., 1995). Dashed lines show corresponding surface roughness for the 500 to 1000 μm fractions of quartz and plagioclase.

only a weak correlation with soil age (S_i = 0.69 to 0.99 m^2 /g, Table 6). Corrected S_i^* values for the primary aluminosilicate fraction were calculated by an equation analogous to Equation (15) assuming that the quartz component has negligible internal porosity. Even with this correction, variability in S_i^* is much less than in λ^* (Table 6) suggesting smaller changes in internal relative to external surface area during weathering. SEM photos of sectioned soil grains (Fig. 10) document that porosity increases with soil age and extent of weathering. However a correlation between porosity increases and greater internal surface area is not straight forward. An increase in internal surface area results if pore diameters increase or if the walls of existing pores roughen. However, if weathering causes a coalescence of many small pores into fewer large pores, the resulting internal surface area could decrease. By definition, internal surface area is that component which is independent of particle volume and includes only that internal surface area that is homogeneously distributed throughout a mineral grain. Preferential pore development, enlargement or roughing near grain surfaces would therefore be assigned to surface-dependent roughness.

In summary, weathering rates are directly correlated with the density of reactive sites on the mineral surface which are exposed to aqueous solution. This reactive surface area is assumed to scale with physical surface area which is measurable by either macroscopic or microscopic means. For naturally weathered soil silicates, the surface roughness factor λ, as defined by the ratio of the BET to geometric surface area, varies between $\lambda = 10^2$ to 10^3. This roughness is attributed both to external surface morphology, which dominates in small grain sizes, and to internal porosity, which is dominant in larger grain sizes.

MINERAL DISSOLUTION RATES BASED ON PRIMARY SILICATE LOSSES

Up to this point in the discussion, the rates of chemical weathering have been defined in terms of changes in elemental or mineral ratios (Eqns. 3 and 5) or in terms of mass normalized with respect to a unit surface area of soil (Eqns. 8 and 9). A more rigorous approach is to quantify weathering with respect to rate constants for individual mineral phases normalized to their specific surface areas. This approach has much more general applicability because soil weathering can then be described by the sum of the rates of the individual minerals present. Equation (1) can be rearranged to define the dissolution rate of a primary mineral phase j in a soil in terms of the reaction rate constant k_j (mol cm^2 s^{-1}). The

$$k_j = \left(\frac{M_j}{\Delta t}\right)\frac{1}{S} \qquad (16)$$

following sections discuss several approaches which can be used to calculated weathering rate constants for minerals in soil environments based on observed losses of primary silicates during soil formation.

Coupling mineral surface area and dissolution rates

As demonstrated by Lasaga (1984), the simplest approach to relating dissolution rates to changes in surface area is through a simple geometric model. For a spherical mineral grain with no surface roughness, the dissolution rate becomes

$$k_j = \frac{r^o - r}{V_j \, \Delta t} \tag{17}$$

where r^o is the initial particle radius and r is the decreased radius caused by dissolution over time Δt. V_j is the molar volume of mineral phase j. The mean lifetime of a weathering particle can be defined as the time Δt required to reduce r to zero. Based on experimental dissolution rate data (Lasaga, 1984; Lasaga et al., 1994) estimated mean lifetimes of 1 mm particles to range from $7.9 \cdot 10^1$ years for wollastonite to $3.4 \cdot 10^7$ years for quartz.

For natural silicates contained in soils, a range of particle sizes and shapes of a given mineral are actually involved in the weathering process. Sverdrup and Warfvinge (1988), in developing a weathering model for soils in the Gårdsjön watershed (Sverdrup, this volume), estimated the total geometric surface area s as the sum of the surface areas of grains in individual size fractions ϕ defined by particle diameter D

$$s = \frac{6M}{\rho\alpha} \sum_{\phi=1}^{n} \frac{f^{\phi}}{D^{\phi}} \tag{18}$$

where α is the average particle sphericity (α=1 for perfect sphere; α = 0.85 to -0.90 for particles with cubic shapes) and f is the fraction of total mass M of particle size ϕ.

Sverdup and Warfvinge(1988) assumed the exposed physical surface area S_t of a mineral phase in a unit volume of soil to be,

$$S = s \, \lambda \left(f_m \, \frac{\rho_j}{\rho_w} \, z \right) \tag{19}$$

where f_m is the weight fraction of the mineral relative to the total soil and ρ_j/ρ_w is the density ratio of the mineral to the soil. The surface roughness λ was estimated from the ratio of the BET and geometric surface areas of freshly crushed particles. The weathering rate constant k_j was then be calculated based on mass differences between bedrock and soil using quartz as a conservative component and a mineral surface area calculated by Equation (19)

$$k_j = \rho_p \left(\frac{x_{qtz,w}}{x_{qtz,p}} \, x_{j,p} - x_{j,w} \right) \left(\frac{1}{S \, \Delta t} \right) \tag{20}$$

Note the terms in brackets are equivalent to the mass balance ratio in Equation (3). The overall equation is comparable to Equation (16) which originally defined the weathering rate constant in terms of relative concentrations of weatherable and non-weatherable soil components. Sverdup and Warfvinge (1988) used Equations (18-20) to estimate soil surface areas and weathering rate constants for microcline, plagioclase and hornblende in soils in the Gårdsjön watershed (Table 7).

Table 7. Comparsion of natural and experimental dissolution rates of selected silicate minerals

	Log Rate k_j ($mol/cm^2/s$)	pH	Environment	Location	Method of Calculation	Surface Area	Age (kA)	Reference
Plagioclase								
Oligoclase	-19.9	4.5-7.0	Soil	Merced, CA	Mineralogy	BET	10-3000	White et al., 1995
Oligoclase	-19.5	4.5-70	Soil	Merced, CA	Solute Flux	BET	10-3000	This paper,
Andesine	-18.7	5	Catchment	Filson Ck., MN	Watershed Balance	Geo	10	Siegel & Pfannkuch, 1984
Oligoclase	-18.5	5.8	Catchment	Bear Brook, ME	Watershed Balance	Geo	10	Schnoor, 1990
Labradorite	-17.7	6.0-7.5	Aquifer	Trout Lake, WI	Groundwater	Geo	10	Kenoyer & Bowser, 1992
Oligoclase	-17.4	4.5-7.0	Soil	Merced, CA	Mineralogy	Geo	10-3000	White et al., 1995
Oligoclase	-17.3	2.0-4.5	Soil Solution	Bear Brook, ME	Solute Flux	Geo	10	Swoboda-Colberg & Drever, 1992
Oligoclase	-17.1	5.6-6.1	Soil	Gardsjon, Sweden	PROFILE model	BET	10	Sverdrup, 1990
Oligoclase	-16.5	6.8	Catchment	Coweeta, NC	Watershed Balance	Geo		Velbel, 1985
Oligoclase	-16.1	5	Catchment	Hartviko, Czech.	Watershed Balance	Geo		Paces,1983
Albite	-16.1	5	Experiment	NA	Dissolution	BET	Crushed	Knauss & Wolery, 1986
Oligoclase	-16.0	5	Experiment	NA	Dissolution	BET	Crushed	Oxburgh et . al., 1994
Albite	-15.9	5.6	Experiment	NA	Dissolution	BET	Crushed	Chou & Wollast, 1985
K-feldspars								
Orthoclase	-20.5	4.5-7.0	Soil	Merced, CA	Mineralogy	BET	10-3000	White et al., 1995
Orthoclase	-19.7	4.5-7.0	Soil	Merced, CA	Solute Flux	BET	10-3000	This paper
K-feldspar	-18.1		Soil	Loess,Il	Etch Pitting (PSD)	Geo	10-15	Brantley et al. 1993
Orthoclase	-17.8	4.5-7.0	Soil	Merced,CA	Mineralogy	Geo	10-3000	White et al., 1995
K-feldspar	-17.3	5.6-6.1	Soil	Gardsjon, Sweden	PROFILE model	BET	12	Sverdrup, 1990
K-feldspar	-17.3	2.0-4.5	Soil Solution	Bear Brook, ME	Solute Flux	Geo	12	Swoboda-Colberg & Drever, 1992
Microcline	-16.8	5.6	Experiment	NA	Dissolution	BET	Crushed	Schweda, 1989
Hornblende								
Hornblende	-20.1	4.5-7.0	Soil	Merced, CA	Mineralogy	BET	10-3000	White et al., 1995
Hornblende	-18.5	2.0-4.5	Soil Solution	Bear Brook, ME	Solute Flux	Geo	10	Swoboda-Colberg & Drever, 1992
Hornblende	-18.1		Soil	Loess,Il	Etch Pitting (PSD)	Geo	10-15	Brantley et al. 1993
Hornblende	-17.6	5.6-6.1	Soil	Gardsjon, Sweden	PROFILE model	BET	10	Sverdrup, 1990
Hornblende	-17.5	4.5-7.0	Soil	Merced, CA	Mineralogy	Geo	10-3000	White et al., 1995
Hornblende	-15.2	4	Experiment	NA	Dissolution	BET	Crushed	Zhang, et al., 1993
Hornblende	-14.7	5	Experiment	NA	Dissolution	BET	Crushed	Sverdrup, 1990

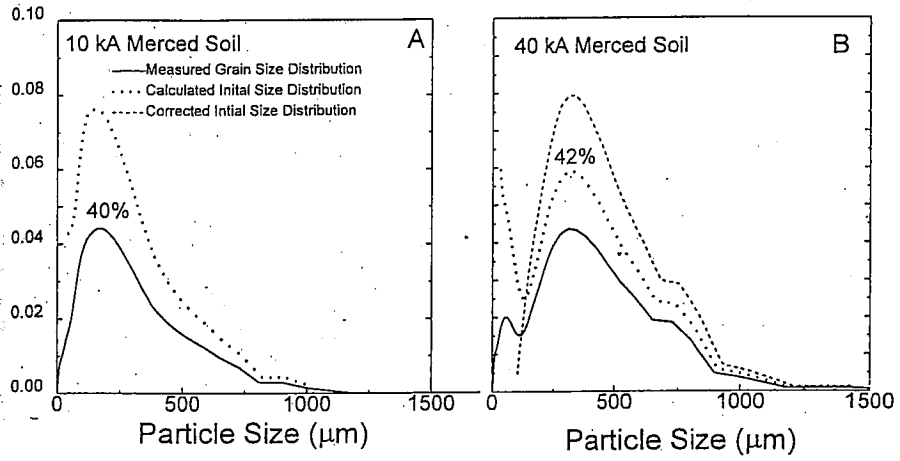

Figure 12. Measured grain size distributions of representative samples of the Merced soils (solid lines) and calculated parent size distributions with (dashed line) and without corrections (dotted lines) for bimodal distribution of fines. Percentages are increases in parent relative to present masses.

Interactive approaches

The above approaches have significant limitations in calculating mineral weathering rates in soils based on mass balances. Although the simple geometric model (Lasaga, 1984) considers the effects of variations in particle mass and size as a function of dissolution, the model did not consider particle size distributions nor the surface roughness of natural mineral grains. The model of Sverdup and Warfvinge (1988) considers grain size distributions but does not consider how particle sizes and surface areas change as a function of mass and volume loss during dissolution. A more inclusive approach to calculating mineral weathering rates in soils is to consider a dynamic model in which a population of grain sizes are considered and for which there is interactive feedback between changes in particle size, surface area, roughness and mass transfer rates (White et al., 1995).

Such a model requires that the initial grain size distribution r^o be known. In soils, such as saprolites, this distribution can be estimated by the mineral size distributions in the parent rock. Under such conditions the surface area and rate constant can be related to changes in grain size distributions in the soil (i e. r^o - r, Eqn. 17). For soils developed on sedimentary deposits, the calculation of changing particle diameter with time requires an inverse solution in which the final rather than the initial grain size distribution is known. As discussed by White et al.(1995) this distribution can be reconstructed by incrementally adding mass back to the present grain-size distribution until the original mass is achieved ($M_j = 1$).

Examples of both present day grain sizes (solid lines) and reconstructed parent grain sizes (dotted lines) for 10 kA and 40 kA Merced soils are shown in Figure 12. Initial calculations of grain size changes with time used complete size distributions measured in the present day soil profiles. Results for the youngest soil showed a relatively symmetric increase in the population of grain sizes from the present distribution for r (Fig. 12A, solid line) to that of the initial parent material r^o (Fig. 12A, dotted lines). However the bimodal distribution of measured grain sizes in the 40 kA Merced soil is greatly accentuated in the calculated parent grain sizes (Fig. 12B). Most of the reconstituted mass was preferentially incorporated into very small grain sizes (< 100 μm) due to their large surface area to mass

ratios. Such pronounced bimodal distributions in the parent material are almost certainly artifacts of the calculation.

The above results point out the importance of grain size on the relative weathering rates and stability of minerals in soils. Due to their large surface area to mass ratios, small size grains of feldspars and other reactive minerals should be rapidly weathered and will not persist in soil environments. In actuality, the small grains in the bimodal size distributions now present in the 40 kA Modesto soil (Fig. 12B) are probably composed of residual quartz grains and fragments of larger feldspar and hornblende grains decomposed by weathering. In additional calculations performed by White et al. (1995), the small grain size fractions were arbitrarily eliminated by smoothing the measured grain-size distributions. The resulting reconstituted size distribution for the parent material (Fig. 12, dashed line) is no longer bimodal and is centered in the sand size fractions which are more representative of weathering processes in granitic terrains.

Calculation of dissolution rates

An interactive dissolution rate model was developed for the Merced soil data (White et al., 1995) that calculates the reaction rate constant k_j (Eqn. 16) based on changes in specific mineral abundance (Fig. 2B), surface roughness (Fig. 11) and changes in particle sizes with time (Fig. 12). A forward approach was employed in which dissolution of each grain size in a sample was sequentially calculated over a number of time steps n from the age of initial deposition to the present. At each time step, the mineral surface area in each size fraction was calculated from the nominal spherical diameter, the appropriate surface area function ($\lambda = 1$ or $\lambda =$ variable), and the mass of mineral in the size fraction. The mass of mineral dissolved in each size fraction during the time step is calculated from the surface area of the size fraction and the dissolution rate. The mass dissolved was then subtracted from the mass of the size fraction, and new nominal diameters for the grains within each size fraction were calculated at the end of the time step. The new diameter was used to calculate the surface area for the next time step, and the process is repeated. Thus, the mass remaining in each size fraction $M^{\phi}_{j,w}$ can be calculated as (White et al., 1995)

$$M^{\phi}_{j,w} = M^{\phi}_{j,p} - \sum_{t=1}^{n} M^{\phi}_{t,j,w} \cdot \varphi_m \cdot S^{\phi}_{t} \cdot k_j \cdot \Delta t \qquad (21)$$

$M^{\phi}_{j,p}$ is the initial mass in the size fraction ϕ, φ_m is the molecular weight of the mineral, and S^{ϕ}_{t} and $M_{t,j,w}$ are the specific surface area and mass of the mineral remaining for size fraction ϕ at time Δt. The proportion of a mineral remaining in a soil profile today R_o is equal to the sum of the mass remaining in each size fraction ϕ divided by the initial mass of the sample,

$$R_o = \frac{\sum_{\phi=1}^{n} M^{\phi}_{j,w}}{\sum_{\phi=1}^{n} M^{\phi}_{j,p}} \qquad (22)$$

Note that R_o is the same term initially defined in Equation (3) but is recast in term of absolute mineral mass rather than concentrations relative to total soil mass. R_o is also used to define actual variations in mineral masses as a function of time as previously shown for the Merced chronosequence data (Fig. 2B). As written, the forward dissolution model (Eqn. 22) requires a specified dissolution rate k_j to calculate the proportion of mineral masses remaining in the soil as a function of age. In weathering studies, these proportions are known and the dissolution rate constants need to be calculated. This problem was solved by finding the

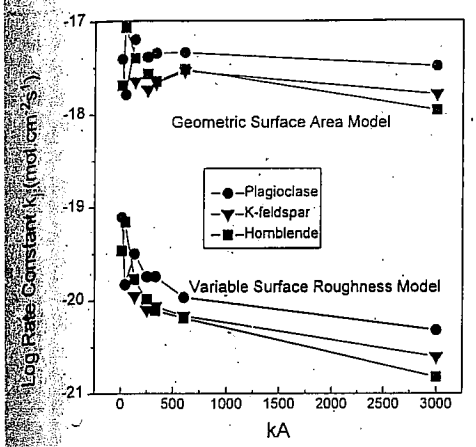

Figure 13. Calculated dissolution rate constants for specific minerals as a function of age in the A horizons of the Merced chronosequence. Rates incorporate geometric surface areas or variable surface roughness (Eqns. 21 and 22).

dissolution rate that yields the closest approximation to the measured mass losses described by R_o (Fig. 2B). Exact solutions of k_j for specific mineral distributions in soils of a given age in the Merced chronosequence were obtained (White et al., 1995). An overall average dissolution rate for each mineral was also determined for the entire chronosequence by minimizing the sum of the squares of the residuals between the predicted and observed mineral abundances. Each soil profile has a different grain-size distribution, which results in a different surface area and a different rate of mass loss. Therefore, this model does not yield a continuous function for mass loss that can be directly interpolated between samples, but rather yields discrete predictions for each individual sample that can be compared with the field observations.

Rates constants calculated from geometric and BET surface area estimates

Geometric and BET surface area measurements are the most commonly used approaches in defining surface areas in weathering rate calculations for natural systems (White and Peterson, 1990). These two scenarios were investigated by White et al. (1995) in relation to surface area effects on weathering rates in the Merced soils. In the first case, geometric surface areas of mineral grains in the model were varied directly with changes in particle diameters and grain-size distributions with time. This approach assumed that the surface roughness was equal to unity (λ=1) and the grains have no internal porosity (S_i=0) (see Eqn. 14). In the second case the BET surface area was interpreted in terms of both an internal surface area, which was assumed constant with time, and an external surface area, which was defined in terms of a roughness factor λ that varied with time (Fig. 11).

Resulting individual dissolution rate constants of plagioclase, K-feldspar and hornblende from the geometric and variable surface roughness models are plotted in Figure 13. The geometric model produces average dissolution rates that are 10^2 to 10^3 orders of magnitude faster than the variable-roughness model. The magnitude of this difference is to a first approximation proportional to the difference between the measured BET and the geometrically-estimated surface areas (Fig. 8). The difference in rates is also dependent on soil age. Based on geometric surface areas, rate constants exhibited no consistent variability with age. In contrast, the variable roughness model predicted that individual dissolution rates decrease by more than an order of magnitude with increasing soil age.

An example of the optimization fit of average dissolution rate constants to mineral distributions in the Merced A horizons is shown in Figure 2. These fits (dashed lines) are

based on the variable roughness model for the mineral surfaces. As indicated, the fit does not produce a single smooth function describing the mineral distributions due to differences in particle size distributions in individual soil profiles. Due to the decrease in k_f with time, a single rate constant fitted to the entire chronosequence underestimated weathering rates in the younger soils and overestimate rates in the older soils. This effect is evident in Figure 2 in which predicted mineral proportions (open symbols) are generally greater than observed proportions (closed symbols) in the younger soils and less than the observed mineral proportions in the older soils.

WEATHERING RATES BASED ON ETCH PIT FORMATION

Changes in mineral surface morphology have been employed to directly quantify mineral weathering rates in soils. As previously discussed, systematic increases in the extent and depth of surface pitting have been observed during weathering of silicate minerals in soil environments (Fig. 6). MacInnis and Brantley (1993) and Brantley et al. (1993) (See Brantley, present volume) have recently developed a pit size distribution model (PSD) which considers the population density of etch pits within a given grain size range during dissolution of a mineral phase. The PSD depends upon the number of pits per unit area, n (cm cm^{-2}) and the growth rate, G (cm s^{-1}) of individual pits. The rate of annihilation of pits, a (s^{-1}), is the rate of coalescence of two pits together, or if the pit stops deepening, the rate at which the pit disappears as the flat surface of the crystal recedes.

Assuming the growth rate is time- and size-independent at constant temperature, a population balance on pits of diameter W (cm) can be written in order to derive the steady-state pit size distribution equation. The following PSD equation results when $dn/dt = 0$, assuming that n_o is the density of etch pits at time 0 and τ is the shear modulus

$$n = n_o \exp\left(-\frac{W}{G\cdot\tau}\right) \tag{23}$$

For these assumptions, a plot of $ln\ n$ against W will produce a straight line with slope $-1/G\tau$ and intercept $ln\ n_o$ (Fig. 14). The PSD model defines the characteristic lifetime, τ, as the reciprocal of the annihilation rate.

A linear PSD plot $ln\ n$ vs. W results when there is a balance between nucleation and annihilation of pits, and where there is size-and time-dependent growth rate of pits. At steady state, PSD coefficients do not change with time; however, linear PSDs are also possible for non-steady-state systems. On the other hand, where annihilation or growth is size dependent, the PSD will not be linear: for example, where coalescence preferentially removes the smallest pits, the PSD may become humped (MacInnis and Brantley, 1993).

The contribution of etch pits to the bulk dissolution rate depends upon the number, density and the rate of dissolution of each pit. By integrating over the PSD, and assuming an average geometry for the pits, MacInnis and Brantley (1993) derived a simple expression for the etching rate of a mineral based upon PSD coefficients. For example, for pit geometries of right pyramids, the contribution of etch pits to the bulk dissolution rate equals

$$R_o = n_o \tan\frac{\theta}{Vj}\cdot G(G\tau)^3 \tag{24}$$

where θ is the pit wall slope.

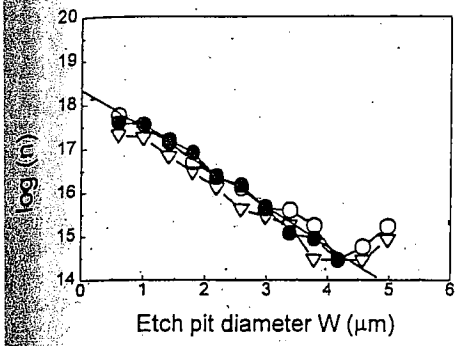

Figure 14. Etch pit size distributions (number of pits n with pit diameter W) for feldspar in Fayatte soil, Illinois. Open circles are upper, solid circles are middle, and triangles are lower soil horizons (from Brantley et al., 1993).

Brantley et al. (1993) analyzed etch pits on loess grains from a 12 kA soil catena from Illinois. For hornblende and potassium feldspar grains, etch pits had not grown to the extent that they had completely coalesced. Where pits have dramatically coalesced, quantification of the pit size distribution is impossible. Figure 14 slows an example of a plot of etch pit width versus number of pits for feldspar from the Fayette soil. Although perfectly linear PSDs were not observed, (typically, distributions exhibited a lack of small pits and an overabundance of large pits), PSD coefficients could be derived for the linear portion of the distribution curves.

By assuming that τ equals the total etching period (12 kA), Brantley et al. (1993) calculated weathering rate constants of log k_j = -18.5 mol cm^{-2} s^{-1} for hornblende grains and k_j = -18.7 2 mol cm^{-2} s^{-1} for K-feldspar. Rates estimated for hornblende were based on consistent crystallographically controlled etch pits, while rates estimated for potassium feldspar were based on irregularly shaped pits. Although little difference in etching rate is observed between soil horizons, the highest etching rates occurred generally in the upper B horizon where the pH was lowest. Etching rates calculated for potassium feldspar were not observed to vary with drainage, while those of hornblende decreased with decreasing drainage. Brantley et al. (1993) argued that decreasing drainage correlates with increasing solute concentration in soil pore waters and increased inhibition of dissolution for the hornblende. Of course, decreased drainage also correlates with lower partial pressures of oxygen in soil waters, which affects hornblende more drastically than K-feldspar.

MINERAL DISSOLUTION RATES BASED ON SOLUTE FLUXES

An alternate approach in determining weathering rates of primary silicates in soils is based on solute fluxes in the soil profile. Conservation requires that the mass of primary mineral phases dissolved in the soil be balanced by the mass increase in secondary minerals minus the loss of mass due to solute fluxes from the profile. The flux Q_k (mol cm^{-2} s^{-1}) for a solute species k through a unit area of a soil profile can be calculated by multiplying the soil water chemical concentration c_k (mol cm^{-3}) by the fluid flux density q ($cm.s^{-1}$). Note that q is equivalent to the rate of water movement through a unit surface area of the soil profile

$$Q_k = q \cdot c_k \tag{25}$$

For a number of chemical species n distributed between different mineral phases m, the mass balance relationship in the soil becomes (Velbel, 1986)

$$\sum_{j=1}^{m} Q_j N_{j,k} = Q_k \qquad k = 1,.....n \tag{26}$$

where Q_j (mol cm^{-2} s^{-1}) is the equivalent flux representing dissolution or precipitation of mineral phase j and $N_{j,k}$ is the stoichiometric ratio of species k in mineral phase j.

The solution to the series of linear equations represented by Equation (26) permits the assignment of portions of solute chemistries and fluxes to a specific mineral phase. Solutions based on "balance sheet approaches" have been used by numerous workers studying chemical fluxes in watersheds (Paces, 1983; Siegal and Pfannkuch, 1984; Velbel, 1985). Use of mass balance models which simultaneously solve the matrix of linear equations, however, permit much greater flexibility in the number of aqueous species and primary and secondary minerals considered. BALANCE (Parkhurst et al., 1982) and NETPATH (Plummer et al., 1991) are two widely used codes which can be used to solve Equation (26).

The reaction rate constant described by Equation (16) for a specific mineral phase j can now be rewritten in terms of solute fluxes which are defined by the product of fluid flux and chemical concentrations (Eqn. 25).

$$k_j = (\frac{M_j}{\Delta t})\frac{1}{S_j} = q\ R_s \sum_{k=1}^{n} N_{j,k}\ c_k^t \tag{27}$$

In Equation (27), c_k^t (mol cm^{-3}) is the concentration of species k produced from weathering of mineral phase j. The measured concentration in the soil solution c_k in Equation (25) is related to c_k^t in Equation (27) such that

$$c_k = c_k^t - c_k^s + c_k^a \tag{28}$$

where c_k^s is the concentration of species k incorporated into secondary mineral phases and c_k^a is the concentration contributed from non-weathering processes such as atmospheric deposition. Equation (28) assumes that the fluid mass is constant and not effected by processes such as evapo-transpiration.

The solute flux is defined in right side of Equation (27) in terms of q (cm s^{-1}) which is equal to the volume of water passing through a unit cross-section area of soil perpendicular to the flow direction. In contrast the rate constant k_j and the mass term M_j are normalized relative to a specific mineral surface area. The conversion factor R_s (cm^2 cm^{-2}) is defined as the ratio of unit area of soil surface area S_s (cm^2) divided by the total surface of S_t (cm^2) of mineral phase j contained in the volume of soil. S_t, in turn, is dependent on the specific mineral surface area S (cm^2 gm^{-1}), the depth of the soil zone z the soil density ρ_w, and the mass fraction of mineral j present in the soil f_m. Therefore, for a unit surface area of soil surface (S_s=1 cm^2)

$$R_s = \frac{S_s}{S_t} = \frac{1}{S} \cdot \frac{1}{\left(z \cdot \rho_w \cdot f_m \right)} \tag{29}$$

Based on the preceding analysis (Eqns. 25-29), the mineral weathering rate k_j can be calculated for a mineral phase if the primary and secondary mineral compositions, solute concentrations and soil water fluxes can be determined.

Table 8. Summary of selected soil water chemistries. Numbers are mean average values with numbers in paratheses as stardard deviations. Units except for pH are in umol.l^{-1}.

Reference	Location	Soil type	Method	pH	Ca	Mg	Na	K	Si	Al
Edmeades et al., 1985	New Zealand	Various	2	6.2 (0.3)	794 (293)	237 (74)	786 (392)	641 (294)	346 (89)	37 (28)
Arocena et al., 1994	Alberta	Sandy Luvisols	2	4.9 (0.7)	670 (618)	165 (83)	79 (28)	294 (246)	235 (170)	105 (65)
Manley et al.,1987	Ontario	Podzols	2	5.1 (0.7)	135 (152)	73 (60)	8 (5)	157 (155)	198 (127)	43 (37)
Campbell et al, 1989	England	Sandy loam	2	6.7	669	226	480	452	210	44
Reynolds et al., 1988	Wales	Stagnopodzols	3	4.3 (0.2)	13 (7)	22 (5)	188 (56)	5 (2)	43 (16)	44 (27)
Katz, 1989	Maryland	Loam/saprolite	3	6.9	133	154	96	5	185	nd
Norfleet et al., 1993	South Carolina	Oxidic loams	3	5.3 (0.5)	12 (9)	10 (10)	85 (52)	34 (22)	105 (69)	2.8 (7)
Hughes et al, 1994	Wales	Stagnopodzols	3, 4	4.3 (0.2)	115 (172)	154 (48)	310 (94)	19 (11)	41 (28)	3 (1)
Soulsby and Reynolds, 1992	Wales	Stagnopodzols	3	3.9 (0.2)	27 (9)	75 (26)	350 (76)	20 (21)	69 (31)	185 (125)
Cronan et al., 1990	New York	Spodosols	3	4.5 (0.2)	45 (8)	11 (3)	32 (11)	21 (13)	121 (33)	58 (18)
Cronan et al., 1990	Tennessee	Ultisols	3	4.9 (0.4)	13 (6)	20 (6)	20 (5)	23 (18)	49 (27)	7 (7.8)
Karathanasis, 1991	Kentucky	Undefined	1	6.3 (0.2)	318 (62)	68 (31)	258 (75)	148 (136)	152 (82)	0 (0)
Ugolini et al, 1999	Japan	Spodosols	3	5.7 (0.6)	36 (32)	24 (19)	126 (90)	118 (167)	87 (67)	3 (3)
White et al (unpublished)	Merced, CA	Utlisols 10-40 k	3	7.1 (0.7)	364 (166)	166 (87)	194 (71)	146. (105)	720 (204)	2 (5)
White et al (unpublished)	Merced, CA	Utlisols 130-330	3	7.0 (0.5)	313 (176)	196 (121)	466 (195)	42 (77)	1150 (570)	4 (8)
White et al (unpublished)	Merced, Ca	Utlisols 600 kA	3	7.2 (0.5)	421 (304)	210 (113)	396 (190)	35 (76)	819 (539)	12 (15)
White et al (unpublished)	Merced, CA	Utlisols 3000 kA	3	7.5 (0.3)	273 (198)	200 (189)	816 (385)	77 (89)	1116 (570)	6 (80)
White et al (unpublished)	Panola. Georgia	Saprolite	3	5.6 (0.2)	52 (44)	56 (31)	91 (40)	15 (8)	212 (69)	53 (220)
White et al (unpublished)	Puerto Rico	Saprolite	3	5.3 (0.7)	16 (20)	32 (18)	189 (77)	2 (6)	118 (88)	5 (9)

Methods of extraction (1) centifuge, (2) centifuge/displacement, (3) suction cup sampler, (4) zero tension sampler

Soil solution chemistry

As described by Joffe (1933), "soil solutions are the blood circulation of the soil body" and as such are the mobile components controlling, as well as reflecting many soil processes, including weathering, chemical equilibrium, ion exchange and nutrient transport. During periods of active recharge, such as precipitation and snow melt events, soil water can be saturated and sampled using zero tension or free drainage lysimeters. More commonly, soil water is present in unsaturated conditions with capillary tension or matrix potential preventing direct sampling under free flowing conditions. The most commonly used techniques for sampling soil water under unsaturated conditions include laboratory-based extraction using centrifugation and immiscible liquid displacement (Campbell et al., 1989; Norfleet et al, 1993) and in situ field techniques such as suction and porous cup samplers (Huges et al., 1994). Accurate characterization of soil solution chemistry is dependent on extraction procedures which produce the minimal amount of physical disturbance to the soil column and the least impact on complex geochemical conditions in the soil waters.

Chemical composition data of unsaturated soil waters pertinent to silicate weathering studies are relatively limited. Selected mean average soil water chemistries cited in the literature, in addition to unpublished data from the Merced, Rio Icacos, and Panola sites, are presented in Table 8. Also included in Table 8 are locations, soil types and sampling methodologies. Mean average soil pHs generally range from neutral to acidic (7.5 to 3.9). In situ pHs are presumable more acidic due to the loss of CO_2 and possible degradation of organic acids during sampling under atmospheric or sub-atmospheric (suction) conditions. Concentrations of major cations range from several tens to hundreds of μmoles, SiO_2 ranges from hundreds to a thousand μmoles and Al ranges from below detection limits to tens of μmoles.

The standard deviations listed in Table 8 approach the mean average chemical concentrations, indicating significant chemical variability in soil solutions. Such differences are in part attributed to spatial variability which influences the hydrological flow path. Heterogeneity in soils is caused by macropores, duripans and lateral flow associated with hill slope processes. Short term temporal variability stems from periods of active recharge during precipitation and snow melt, which dilutes the soil solution, followed by periods of evapo-transpiration, which tend to concentrate soil solutions.

Longer term chemical variability in soil solutions generally reflects the intensity of soil weathering and the mineral compositions in the soil profile. Solute concentrations often increase with increasing depth in soil profiles, reflecting longer fluid residence times and greater inputs from the weathering of silicate minerals. The effect of soil age on weathering inputs is demonstrated by the bivalent/monovalent chemical ratios in soil solutions of various soil profiles in the Merced chronosequence. As shown in Figure 15, the Ca/Na ratios clearly decrease from approximately 4 in the youngest Modesto soils to less than 0.3 in the oldest China Hat soils. This decrease corresponds to a decrease in the more weatherable plagioclase and hornblende minerals which contain abundant bivalent cations relative to alkali feldspar, which dominants weathering reactions in the older soils. In this case, the evolution of the soil solution chemistry clearly corresponds to the weathering sequence of the minerals in the soils.

Comparison of soil solution and watershed chemistry

Most watershed studies, which have estimated soil weathering rates, assume that surface discharge chemistry reflects the soil water chemistry. However few studies have attempted to make direct chemical comparisons or to address where in the soil profile

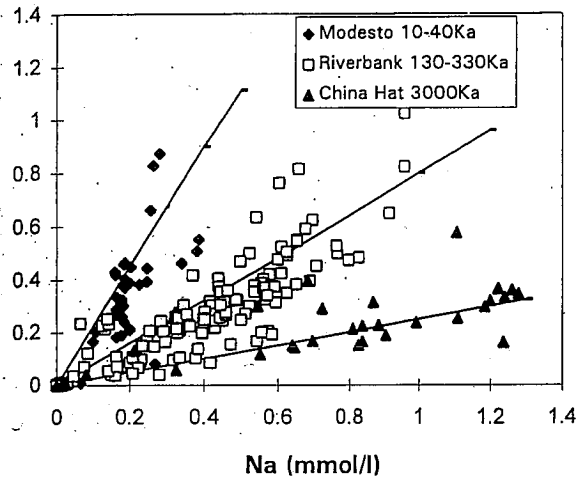

Figure 15. Ca-Na ratios in soil solutions of different ages in the Merced chronosequence. Diagonal lines are regression fits to data.

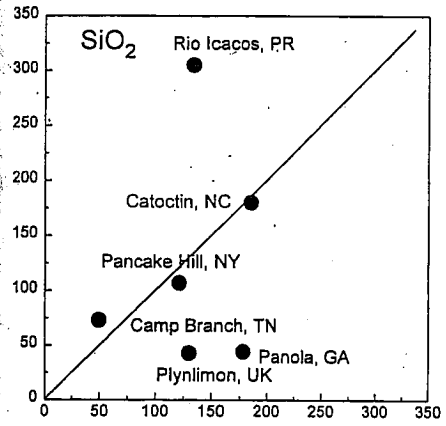

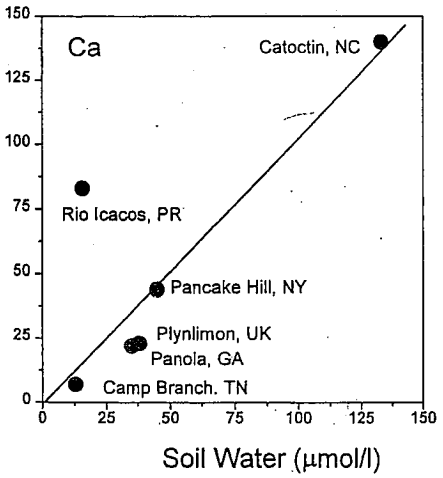

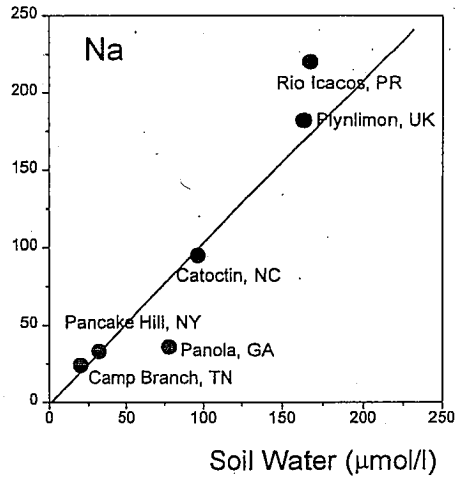

Figure 16. Comparison of average soil solution compositions with corresponding mean annual surface discharge chemistry in selected watersheds.

weathering actually occurs. The average soil solute SiO_2, Ca and Na concentrations reported in Table 8 are compared to mean annual surface water discharge concentrations for corresponding watersheds in Figure 16. The one-to-one solid diagonal lines represent the situation in which the mean soil solution chemistry is directly reflected in the average stream chemistry. As indicated this assumption appears valid for several of the watersheds.

However significant discrepancies between soil and surface chemistries are also apparent. For example, SiO_2 and cation concentrations in Panola watershed are generally lower in the surface water relative to that in the soil water (Fig. 16). This discrepancy is related to significant surface runoff from exposed bedrock in the watershed. Rapid surface runoff, reflecting low dissolved solids, dilutes the surface water discharge relative to the more concentrated weathering input from soil waters. In contrast, average surface discharge water in Rio Icacos watershed is more concentrated than the soil water chemistry. As indicated by the previous discussion of mass balances, weatherable minerals are almost totally depleted in the Rio Icacos saprolite (Fig. 1). Most weathering of granitic mineralogy occurs at a narrow interface between the bedrock and soil zone. Weathering of this interface therefore contributes to higher silica and cation concentrations in the surface water discharge relative to weathering in the overlying sapolite.

Equilibrium controls on soil solution chemistry

The precipitation of secondary minerals, most commonly clays and Al and Fe hydroxides and oxides, is expected to strongly influence the weathering signature contained in soil solutions and to impact mass balance calculations (Eqns 27- 28). For example, SiO_2 is the major chemical species most directly related to weathering reactions. Silica is not contributed from atmospheric precipitation nor is aqueous SiO_2 extensively modified by soil ion exchange processes and biological uptake. However SiO_2 concentrations are strongly affected by precipitation of clay minerals. Kaolinite is the most commonly reported weathering product of silicate rocks in soils. The weathering reaction for plagioclase can be represented as

$$[NaAlSi_3O_8]_{albite} + 1.5\ H_2O + CO_2 \rightarrow 0.5[Al_2SiO_2O_5(OH)_4]_{kaolinite} + Na^+ + HCO_3^- + 2H_4SiO_4$$

The stoichiometry of the above reaction requires the aqueous release of two moles of SiO_2 for every mole incorporated with Al in the solid phases. If gibbsite forms in the soil, 3 moles of SiO_2 will be released and if smectites forms, less than 2 moles of silica will be mobilized. The actual silica concentrations in soil solutions depend strongly on equilibrium with secondary mineral phases.

One common approach to determine mineralogical controls on solution chemistry is the use of activity diagrams (Garrels and Christ, 1965). The above reaction can be characterized by plotting the aqueous activity of H_4SiO_4 in the soil solution versus the ratio of Na^+/H^+. Activity diagrams for the systems Na_2O-Al_2O_3-SiO_2-H_2O in addition to systems K_2O-Al_2O_3-SiO_2-H_2O and CaO-Al_2O_3-SiO_2-H_2O are shown in Figure 17. The soil solution data from the references tabulated in Table 8 are plotted based on the assumption that activities are comparable to chemical concentrations. In terms of SiO_2 phases, soil solutions appear generally unaffected by quartz solubility i.e., chemical concentrations (activities) plot both above and below quartz solubility (Fig. 17, left-hand vertical dashed line). In contrast, maximum aqueous SiO_2 concentrations in soil waters appear to be limited by the precipitation of amorphous silica (Fig. 17, right-hand vertical dashed line) which commonly is associated with the formation of duripans and fragipans in soils (Karathanasis, 1989).

Most of the soil solution data fall within the kaolinite stability field (Fig. 17), a

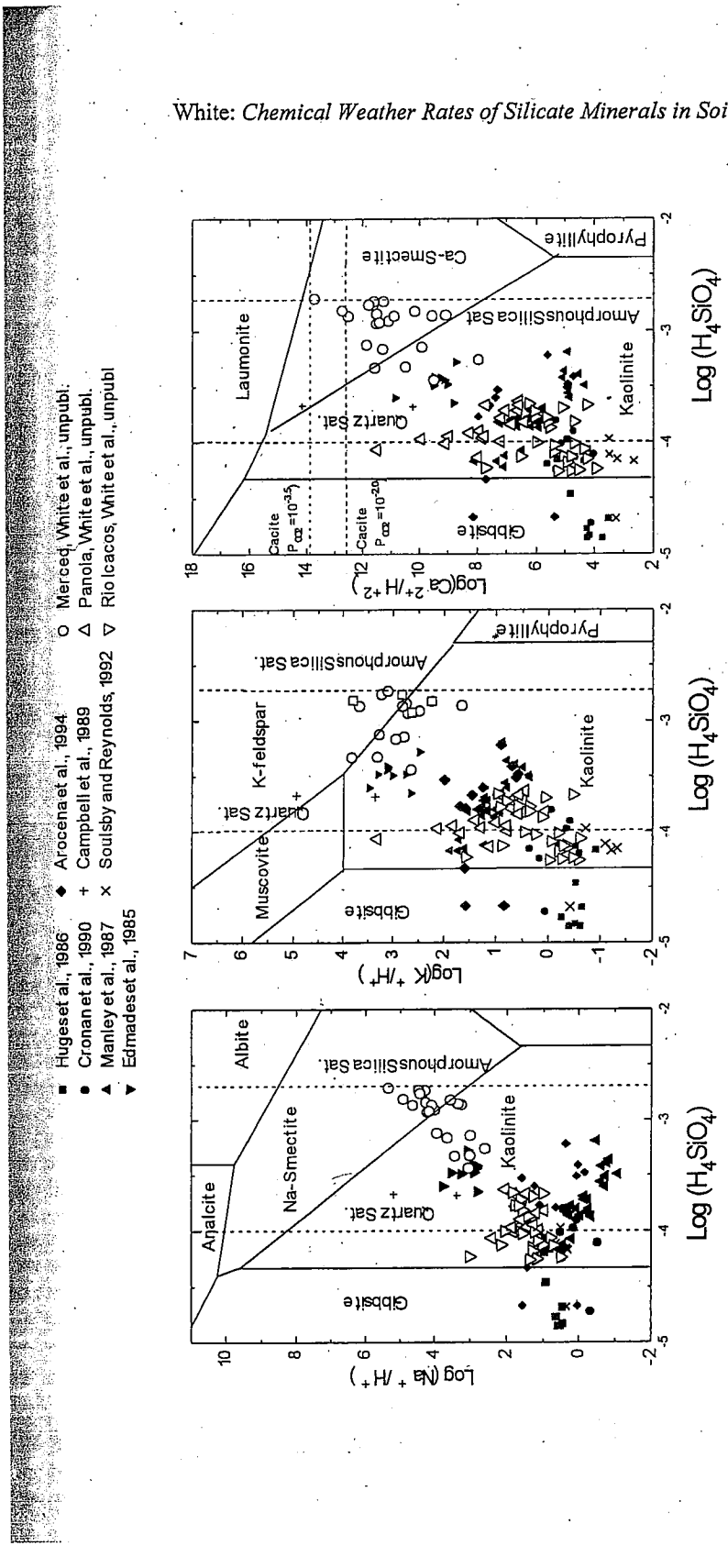

Figure 17. Soil solute concentrations (Table 8) plotted on mineral stability fields for the systems Na_2O-Al_2O_3-SiO_2-H_2O, K_2O-Al_2O_3-SiO_2-H_2O and CaO-Al_2O_3-SiO_2-H_2O.

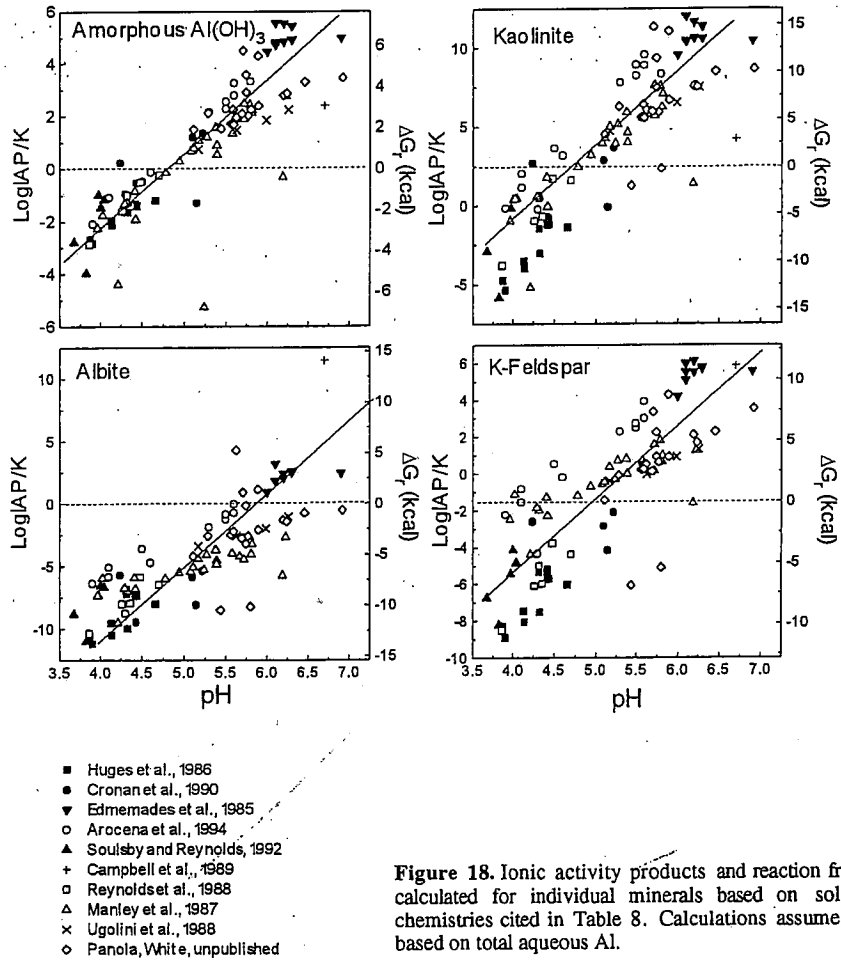

Figure 18. Ionic activity products and reaction free energies calculated for individual minerals based on solution soil chemistries cited in Table 8. Calculations assume speciation based on total aqueous Al.

situation previously observed for activity diagrams developed for other soil solution studies (Manley et al., 1987 ; Katz, 1989). Kaolinite is also the most common clay mineral forming in association with common silicate rocks such as granite. The diagrams indicate, however, that some soil solutions are undersaturated with kaolinite. Such a situation is evident in the Rio Icacos soils where kaolinite is actively undergoing dissolution in the upper horizons of the soil profile. Soil waters with high solute concentrations cross over into the Na and Ca smectite stability fields (Fig. 17) suggesting that smectite formation also occurs in some soils. High Ca^{2+}/H^{+2} ratios in some soils also indicate that soil solutions saturate with calcite which is supported by the presence of calciche formation. The activity diagrams also suggest the some soil solutions are approaching saturation with respect to primary silicate minerals such as K-feldspar.

The stability of both secondary and primary mineral phases can also be predicted directly from solubility calculations. The mineral solubility product is defined as K and the corresponding aqueous ionic activity product is defined as IAP. Based on strict thermodynamic interpretation, when $IAP/K = 1$ the free energy of reaction is zero $\Delta G_r = 0$

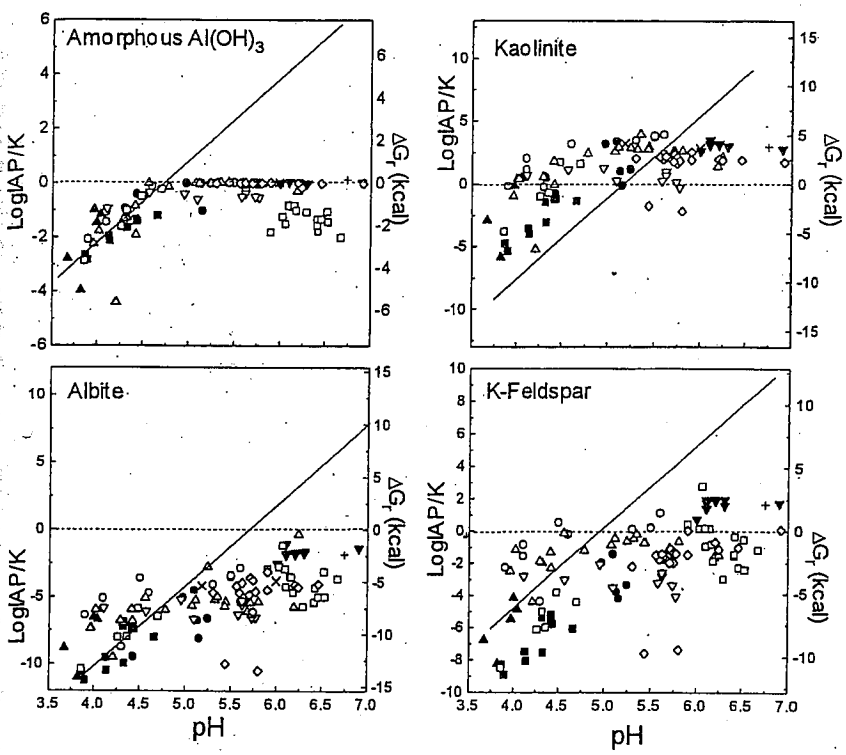

Figure 19. Ionic activity products and reaction free energies calculated for individual minerals based on soil solution chemistries cited in Table 8. Calculations assume that Al concentrations are controlled by gibbsite saturation at measured pH. Symbols as in Figure 18.

and the mineral phase is in equilibrium with the soil solution. When $IAP/K < 1$, then $\Delta G_r < 0$, and the mineral will dissolve. When $IAP/K > 1$, then $\Delta G_r > 0$ and the mineral will precipitate. Under ambient soil solution conditions, the above thermodynamic interpretation is strongly modified by kinetic restraints on the reactions as will discussed in a following section.

Saturation states for soil waters (Table 8) were determined using the SOLMINEQ 88 chemical speciation code (Kharaka et al., 1988). Minerals included in the calculations were gibbsite and kaolinite, secondary phases which commonly precipitate from soil solutions, and albite and K-feldspar, phases that commonly dissolve. *IAP/K* values based on total Al analysis indicate very wide ranges in solution saturation for the mineral phases (Fig. 18). At low pH, the solutions are generally unsaturated (below the dashed saturation line) and at near neutral pH, the solutions are over saturated (above the dashed saturation line). The maximum calculated *IAP* values suggest that the soil solutions at near neutral pH exceed gibbsite saturation by 5 orders of magnitude and kaolinite by 15 orders of magnitude.

The plot of pH versus *IAP/K* for the soil solution data approximate a slope of 1 to 3 (diagonal lines; Fig. 18) even in supersaturated solutions. This slope is proportional to a direct dependence of *IAP* on H^+ activity if the Al concentration is approximately constant and independent of pH. Precipitation of gibbsite or kaolinite is not reflected in this consistent ratio even though these minerals commonly occur as secondary weathering products in soils.

This discrepancy results from difficulties in the measurement of Al at low concentrations, particularly at near-neutral pH. Dissolved Al in such pore waters are present in a number of forms including inorganic, organic and polymeric species (Huges et al., 1994). Complexation, coupled with common problems associated with sampling, filtration and analysis, often result in significant over-estimation of Al concentrations equilibrated with Al-containing minerals (Hem, 1985).

One approach to correct for analytical measurements and speciation of Al in thermodynamic calculations is to assume that Al is controlled by saturation with a simple $Al(OH)_3$ phase such as gibbsite (Wesolowshi, 1992). This approach is supported by detailed analyses of Al in soil waters which suggest that monomeric inorganic Al concentrations at near-neutral pH is controlled by amorphous or microcrystalline gibbsite saturation (Karathanasis, 1989; Norfleet et al., 1993). Using this approach, the *IAP* values for gibbsite, kaolinite, albite and K-feldspar were recalculated by assuming that the maximum *IAP* for $Al(OH)_3$ is limited by gibbsite saturation at any given pH. This was achieved in the SOLMINEQ.88 program by back-titrating excess Al from the analysis until gibbsite saturation was achieved. These results (Fig. 19) indicate that the increase in *IAP* becomes truncated at gibbsite saturation at pHs above approximately 4.5. These limiting values on Al concentrations produce more realistic results in terms of saturation with respect to the other mineral phases.

Role of solute chemistry and reaction affinity

From elementary thermodynamics, the free energy of the weathering reaction can be defined as

$$\Delta G_r = RT(\log IAP - \log K) \tag{30}$$

Transition state theory (TST) can be used to relate the kinetic rate k_j to this reaction affinity (Lasaga, 1981) (Also see this volume),

$$k_j = -k_o \left(1 - \exp\left(\frac{n\Delta G_r}{RT}\right)\right) \tag{31}$$

where n is the reaction order. In Equation (31), k_j is defined as the net reaction rate between precipitation and dissolution reactions at the mineral surface. For dissolution reactions, values of ΔG_r and k_j are negative and for precipitation reactions ΔG_r and k_j are positive. At $\Delta G = 0$ the rates of dissolution and precipitation are equal. Equation (31) predicts that far from thermodynamic equilibrium, the dissolution or precipitation rate will be independent of ΔG_r and equal to a constant rate ($k_j = k_o$),whereas at progressively closer to equilibrium, ΔG_r will exert an increasingly stronger effect on the overall reaction rate ($k_j < k_o$). *IAP/K* values reported in Figure 19 suggest that kaolinite precipitates out of solution at relatively constant supersaturation approximately 100 times above *K*. This *IAP* corresponds to an average ΔG_r value of approximately 3 kcal. The effect of increasing supersaturation on the increasing rates of kaolinite precipitation was been investigated experimentally at elevated temperatures (80°C) (Nagy et al., 1991; Nagy et al., 1993) (also see Nagy, this volume). Assuming comparable relationships between ΔG_r and rates at lower temperature, these studies suggest that kaolinite may be precipitating out of soil solutions at significantly more rapid rate than if the solutions were less saturated.

The extent of solution supersaturation and therefore the rate of precipitation of kaolinite from soil solutions is controlled in large measure by the rates of Al and SiO_2 release from

weathering of primary silicates such as albite and K-feldspar. Based on strictly thermodynamic considerations (Eq. 30), these phases should not dissolve in solutions that exceed their saturation state. This conclusion may be tempered somewhat for soil solutions by kinetic restraints which prevent reprecipitation of these phases from solutions which become supersaturated due to concentration by evapo-transpiration and other processes. As indicated however, soil waters generally remain undersaturated with respect to albite over the entire soil water pH range and saturate with respect to K-feldspar only near neutral pH.

In summary soil solutions reflect both input from weathering processes and may influence weathering rates by controlling both precipitation of secondary minerals and the rates of primary mineral dissolution.

Soil Water Hydrology

The determination of the soil water flux density q is required in order to calculate mineral weathering rates based on soil water chemistry (Eqns. 25 and 26). A general review of unsaturated zone hydrology is beyond the scope of this paper and the reader is referred to texts on the subject such as Hillel (1982). Briefly the flux density per unit area of soil S_s can be defined by the Richards equation (Richards, 1931)

$$q = -K_m \nabla H \tag{32}$$

where K_m is the unsaturated hydraulic conductivity and ∇H is the hydraulic gradient. Equation (32) is equivalent to Darcy's law with the complication that K_m is dependent on degree of saturation or moisture content of the soil (m = volume water/volume soil).

When the soil is saturated, all of the pores are water filled, so that continuity and hence conductivity are maximal. When the soil desaturates, some of the pores become air filled and the conductive portion of the soil cross sectional area decreases correspondingly. The first pores to empty are the largest ones which are the most conductive thus leaving water to flow only in the smaller pores increasing tortuosity. For these reasons, the transition from saturated to unsaturated flow in soils generally entails a steep drop in hydraulic conductivity. An example of the effect of moisture content on the hydraulic conductivity K_m for a silty loam developed on eolian deposits in Central Washington is shown in Figure 20 (Globus and Gee, 1995). As indicated, a decrease in moisture content from 0.27 to 0.05 causes 4 orders of decrease in K_m

In addition to changes in the hydraulic conductivity, the hydraulic gradient ∇H is also dependent on variations in soil saturation. The change in head with soil depth can be described such that

$$\frac{dH}{dz} = \frac{dh_g}{dz} + \frac{dh_p}{dz} \tag{33}$$

h_g is the gravitational head at any point and h_p is the head related to the matrix potential or suction due to the capillary affinity of water of the soil mineral surfaces. Determinations of fluid, and conversely chemical fluxes in soils based on Equations (30) and (31), are difficult for most soil conditions due to the non-linear dependence of conductivity and head potentials on moisture content and matrix potential.

Estimating rates of fluid flow

Several approaches can be used to overcome the complexities of unsaturated flow and

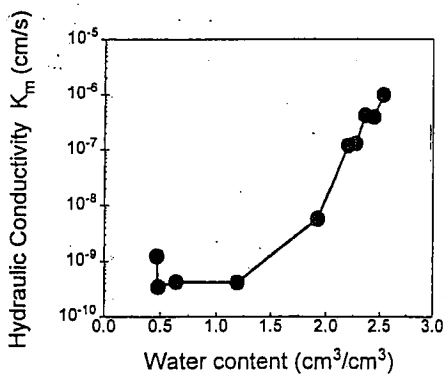

Figure 20. Hydraulic conductivity K_m versus water content for the Palouse silt loam, Central Washington (after Globus and Gee, 1995).

to estimate water fluxes through soils. One approach is to not consider the hydrologic details of soil zone at all and simply calculate soil water fluxes from simple input-output (I/O) balances. As previously mentioned and discussed in greater detail by Drever (this volume) watershed I/O balances is one such approach to calculate both water and solute fluxes through the soil zone. This approach relies on the assumption that discharge from the watershed reflects percolation through the soil zone and that the spatial variability of the watershed soils can be either be characterized or ignored.

The fluid flux can also be calculated from a one dimensional I/O water balance in a soil profile where q is assumed equal to the difference between precipitation *P* (cm/y) and evapo-transpiration ET (cm/yr) which occur through the upper boundary of the soil profile

$$q = P - ET \tag{34}$$

Because most evapo-transpiration in soils occurs via plant respiration, direct estimates of *ET* require detailed measurements which are specific to soil and vegetation types. *ET* can also be indirectly estimated by comparing the concentration c_k^a of a chemical species that is contributed solely from precipitation to its concentration c_k in the soil zone which has undergone concentration by ET. This is equivalent to assuming that c_k^l and c_k^s are zero in Equation (28) and the mass of fluid is no longer conservative. Under steady state conditions this relationship becomes (Erikkson and Kunakasem, 1969)

$$q = P \cdot \frac{c_k^a}{c_k} \tag{35}$$

Finally, estimates of fluid flux can be made based on fluid residence times in the soil profile. Several age dating techniques including ^3H and ^{36}Cl have been successively employed in the age dating relatively young soil-waters and in estimating hydraulic conductivity (Allison et al., 1994).

The alternate approach to estimating soil water fluxes is to apply simplifying assumptions to Richards equation (Eqns. 32 and 33) for specific soil environments. Compared to the simple I/O models discussed above (Eqns. 34 and 35), such an approach provides greater information on coupled processes that link soil mineral weathering with soil hydrology. A special case predicted by the Richards equation relates to unsaturated zone flow under conditions of constant matric potential or capillary pressure within a vertical section of a soil profile (i.e $dh_p/dz = 0$) . In such a case $dh_g/dz = -1$ (Eqn. 31) and the flux

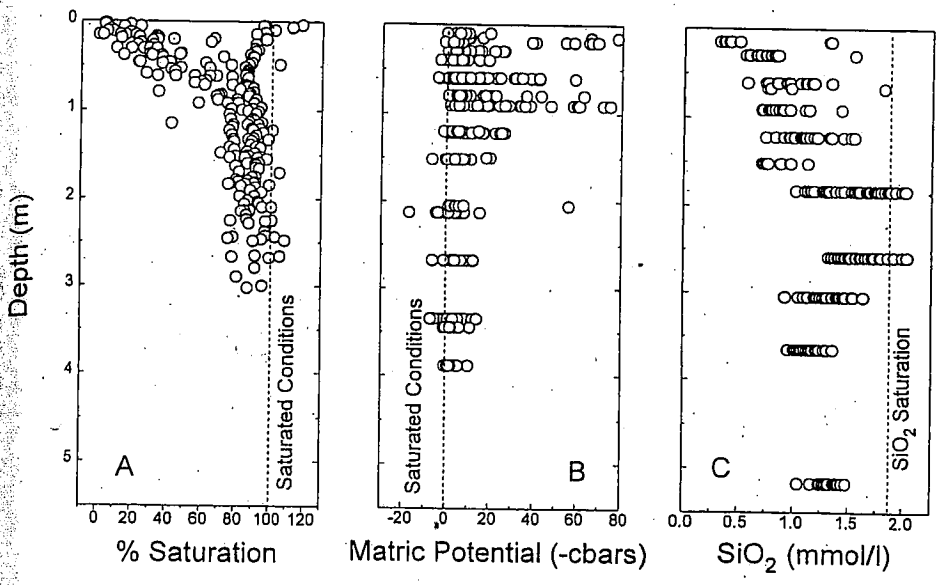

Figure 21. Soil water saturation (A), matrix potential h_p (B), and dissolved SiO_2 (C) in the Riverbank soil profile, Merced, California.

density becomes directly proportional to the hydraulic conductivity

$$q = -K_m \tag{36}$$

One situation in which the flux and hydraulic conductivity may become equal (Eqn. 36) is when an impeding layer is present within a soil column. The effect is to decrease the hydraulic potential in the profile under the impeding layer and to stabilize the development of suction in the subsoil (i.e. $dh_p/dz \rightarrow 0$). This condition, when produced under experimental field conditions, has been proposed as a method for determining unsaturated hydraulic conductivity (Hillel and Gardner, 1970). Such impeding layers are also a common occurrence in many natural soils in the form of caliche layers, duripans and fragipans. Such soil textures are commonly formed by precipitation of silica, iron oxyhydroxides and clay minerals during cyclic wetting and drying of shallow zones of the soil profile (Karathanasis, 1989). A common feature is low hydraulic conductivity within these layers which often results in seasonal saturated or near saturated conditions in overlying portions of the soil profile and relatively steady state unsaturated conditions in the underlying portions.

Example of estimation of soil water flux

In this section, the hydraulic characteristics of the 250 kA Riverbank soil of the Merced chronosequence are used to illustrate methods for estimating hydraulic conductivity K_m and fluid fluxes q. The variations in moisture content (% saturation), matrix potential and SiO_2 concentrations are shown as functions of depth in Figure 21. Soil moisture was calculated from measured gravimetric water content, an average measured soil density of $\rho_w = 1.85$ g cm^{-3} and an assumed mineral density of $\rho_p = 2.65$ g cm^3. In the upper 1 m part of the soil profile soil saturation approaches 100% during wet conditions in the winter and 0% during dry conditions in the summer (Fig. 21A). Below approximately 1 m, the moisture content

Table 9. Solute data for the Riverbank soil profile, Merced, CA.

Element	Precipitation P (mmol l^{-1})	Precipitation Std dev.	Soil Water[1] c_k (mmol l^{-1})	Soil Water Std dev.	Fluid Flux[1] q (cm s^{-1})	Solute Flux[1] Q_k (mol cm^{-2} s^{-1})
Na	0.037	0.002	0.539	0.023	7.6E-08	3.8E-11
K	0.001	0.001	0.032	0.001	7.6E-08	2.4E-12
Mg	0.030	0.012	0.125	0.005	7.6E-08	7.2E-12
Ca	0.018	0.009	0.188	0.005	7.6E-08	1.3E-11
Si	0.006	0.002	1.340	0.024	7.6E-08	1.0E-10

[1]soil water data is at 5.2 m in the soil profile

Table 10. Mineral dissolution and precipitation rates in the upper 5.6 m of the Riverbank soil, CA

Mineral	Formula	Mass (mmol l^{-1})	Fluid Flux q (cm s^{-1})	Mineral flux Q_j (mole cm^{-2} s^{-1})	Mineral rate k_j (mol $cm^{-2}s^{-1}$)
Plagioclase	$Na_{0.684}Ca_{0.316}[Al_{1.316}Si_{2.684}O_8]$	0.566	7.60E-08	4.30E-14	3.47E-20
K-feldspar	$K_{0.0775}Na_{0.225}[AlSi_3O_8]$	0.468	7.60E-08	3.56E-14	2.24E-20
Biotite	$K_{0.958}Na_{0.387}(Mg_{1.686}Fe_{1.1968}(Al_{0.793})[Al_2Si_{6.22}](OH)$	0.063	7.60E-08	4.79E-15	nd[1]
Kaolinite	$[Al_2Si_{6.22}0](OH)_4$	-0.656	7.60E-08	-4.99E-14	nd
Silica	SiO_2	-0.432	7.60E-08	-3.28E-14	nd
Goethite	FeOOH	-0.095	7.60E-08	-7.22E-15	nd

[1]not determined

becomes relatively constant with an average saturation of 85%. The corresponding matrix potentials were measured with nested tensiometers. A matrix potential of zero corresponds to saturated conditions whereas high matrix potentials correspond to low moisture contents. As in the case for moisture content, the upper soil zone exhibits significant variations in matrix potentials between wet and dry seasons, while below 1 m, the matrix potential becomes nearly constant throughout the year with an average potential of approximately 10 cbar (Fig. 21B).

These relatively steady state hydrologic conditions occur below a silica duripan which is pervasive between 1 to 2 m depth in the older soils of the Merced chronosequence. The formation of this layer corresponds to high SiO_2 solute concentrations which at these depths approach silica gel saturation (Fig. 21C, dashed vertical line). Resulting SiO_2 gel precipitation is achieved by concentration through evapo-transpiration of soluble SiO_2 originally derived from silicate weathering. With time, the formation of such duripans at shallow depths become self perpetuating, whereby evapo-transpiration produces additional silica precipitation which in turn leads to lower permeability which furthers the effects of evapo-transpiration.

The above observations (Fig. 21) suggest the rate of soil water movement is controlled principally by rates of slow infiltration through the duripan. Above this zone, the hydraulic head is strongly influenced by cyclic seasonal rainfall and ET, while below this interface, the head is controlled principally by gravimetric flow (dh_f/dz =0, Eqn. 33). Under such conditions, the soil water flux density can be approximated by a constant conductivity ($q = K_m$, Eqn. 36). A single saturated conductivity measurement made on in situ core from the Riverbank duripan, using a biased falling head setup, produced a value of $1 \cdot 10^{-7}$ cm s^{-1}. This is comparable to the saturated conductivity reported by Globus and Gee (1995) for the Palouse soil (Fig. 20) and is higher than expected for less saturated soil conditions.

An alternative approach is to calculate the fluid flux q through the profile based on Cl concentrations. Under such steady state conditions, q and therefore k_s can be calculated from Equation (35). Precipitation chemistry was analyzed for samples periodically taken from open precipitation collectors which represented both wet and dry fall inputs. The average atmospheric Cl concentration over a 4 year time period was $c_{Cl}^a = 25 \pm 18$ μmol l^{-1}. Cl distributions in the soil pore waters exhibit a similar trend as SiO_2 (Fig. 21C). In the deeper unsaturated zone below the duripan, seasonal variations damped out. At a maximum measured depth of 5.6 m, the average soil water Cl concentration is $c_{Cl} = 308 \pm 109$ μmol l^{-1}. Based on these estimates, approximately 8% of the precipitation was recharged through the 5.6 m of soil while 92% was lost to *ET*. As previously indicated, annual mean precipitation at the Merced site is P = 30 cm yr^{-1}. Substituting these values into Equation (35) results in a fluid flux through the system of $q = 2.4$ cm. yr^{-1}. This corresponds to a unsaturated hydraulic conductivity $K_m = 7 \cdot 10^{-8}$ cm s^{-1} (Eqn. 36). As expected, this value is somewhat lower than the saturated hydraulic conductivity measured experimentally.

Soil mineral weathering rates based on solute fluxes

The determinations of the chemical concentrations and fluid fluxes allows us to now calculate solute fluxes through the Riverbank soil profile (Eqns. 27 and 29). Table 9 lists average chemical concentrations for major cations and silica measured over a 4 year period in precipitation and at 5.6 m depth in the Riverbank soil. The difference in these concentrations is assumed to correspond to the chemical concentration contributed from chemical weathering (Eqn. 28; $c_k - c_k^s$). The standard deviations of the soil water solutes are small (0.01 to 0.024 mol l^{-1}). This suggests, as shown in the examples for SiO_2 (Fig. 21C), that chemical fluxes in the deeper unsaturated zone are relatively constant over time. The

solute fluxes calculated by Equation (27) were found to range between $Q_k = 2 \cdot 10^{-12}$ mol cm^{-2} s^{-1} for K to $Q_k = 1.0 \cdot 10^{-10}$ mol cm^{-2} s^{-1} for SiO_2.

The solute concentrations for precipitation and soil water (Table 9) were used as input to the NETPATH program to calculate corresponding masses of mineral dissolved in the first 5.6 m of the soil zone. Mineral stoichiometries used in the model were previously determined for the Merced soils (White et al., 1995). Attempts to constrain the model using K were unsuccessful apparently due to the fact that dissolved K concentrations do no realistically reflect weathering reactions. K in the Merced soils is probably dominated by ion exchange processes and influenced by nutrient cycling in the vegetative cover.

NETPATH output, in terms of reacted mineral masses and weathering fluxes are tabulated in Table 10. The mass flux of each mineral phase per unit of surface area of soil can be calculated in a manner analogous to that for solute fluxes (Eqn. 25) by multiplying mineral concentrations times the fluid flux density. Positive values correspond to mineral dissolution and negative values to mineral precipitation. Approximately 60% of the original mass of plagioclase and 18% of the K-feldspar have dissolved between Riverbank time and the present (250 kyr) These results are in agreement with the loss of these phases previously calculated from solid state mass balances (Fig. 2B). The NETPATH output predicts only minor dissolution of biotite which is in agreement with its observed resistance to weathering in the soil profiles. The model was found not to converge with calculations involving hornblende apparently due to errors in estimating mineral stoichiometry and/or problems with K balances. The precipitated secondary mineral phases (Table 10, negative values) are kaolinite, amorphous silica, and goethite which is consistent with the observed secondary mineralogy in the soil sequence.

The final step in calculating the mineral dissolution rate k_j is to normalize the mineral flux Q_k to the mineral surface S rather than the soil surface area S_s. From Equations (26-29)

$$k_j = R_o \cdot Q_j \qquad (37)$$

R_o was determined by Equation (29), where the specific surface areas of plagioclase and K-feldspar were 0.46 and 0.94 m^2 g^{-1} (Table 5), and the respective mineral wt fractions in the Riverbank soil are $f_m = 0.26$ and 0.16 (Fig. 2B). The total soil depth is $z = 5.6$ m and the soil density is $\rho_w = 1.85$ g cm^{-3}. Combining these parameters in R_o with the mineral flux values in Table 10 resulted in mineral dissolution rate constants log k_j = 19.5 mol cm^{-2} s^{1} for plagioclase and log k_j =-20.5 mol cm^{-2}.s^{-1} for K-feldspar (Eqn. 37). The corresponding rates previously derived from the mineral mass balance model (Eqns. 21 and 22) were log k_j = -19.9 mol cm^{-2} s^{-1} for plagioclase and -19.7 mol.cm^{-2}s^{-1} for K-feldspar (Table 7). The degree of similarity in the rates is remarkable considering that the number of assumptions used in both models. This similarity also suggests that current weathering rates, characterized by solute fluxes, must be comparable to average rates impacting weathering over the 250 kyr of soil development.

INTERPRETATION OF WEATHERING RATE CONSTANTS IN SOILS

The following discussion will compare the weathering rate constants derived from examples described in the previous sections with k_j values reported in the literature for soils and for selected experimental studies for minerals common to soils. Table 7 tabulates weathering rate constants k_j in increasing order of reaction for plagioclase, K-feldspar and hornblende. These minerals are common in soils developed on crystalline bedrock such as granite. Rates were determined by various methods including mineralogical mass balances (White et al., 1995), etch pit distributions (PSD model, Brantley et al., 1993), soil solute

fluxes (Swoboda-Colberg and Drever, 1992; present paper), watershed solute balances (Paces, 1983; Velbel, 1985; Siegal and Pfannkuch, 1984; and Schnoor, 1990) and the integrated PROFILE model (Sverdrup, 1990) (see Sverdrup, this volume). Also included are selected rates based on experimental mineral dissolution. The rate constants range from log k_j = -19.9 to -15.9 mol cm^{-2} s^{-1} for plagioclase, from log k_j =-20.5 to -16.8 mol cm^{-2} s^{-1} for K-feldspar and from log kj =-20.1 and -15.2 mol cm^{-2} s^{-1} for hornblende.

An important observation apparent from the tabulation is that the differences in rate constants for individual minerals greatly exceeds any apparent difference in weathering rates for different minerals. Blum (1994) previously noted that the experimental dissolution rates of albite and K-feldspar in the acid and neutral pH range are indistinguishable. Comparable differences between mineral phases in natural systems are also generally small (Velbel, 1993). In the Merced soils, plagioclase weathers only 2.5 times faster and hornblende only 5.5 times faster than K-feldspar. The time-dependent distribution of residual minerals in the Merced soils, however, puts very tight controls on the magnitude of these rate constants. A 50% increase or decrease in observed residual mineral abundances, such as reported in Figure 2B, changes the calculated reaction rate by only a factor of ±2. Such small differences in rates clearly fall below the resolution of the range in rate constants reported in Table 7.

In general, calculated rates for natural systems are significantly slower than for the experimental studies. Several researchers have previously documented that natural weathering rates appear one to three orders of magnitude lower than experimentally predicted rates (Claassen and White, 1979; Paces, 1983; Swoboda-Colberg and Drever, 1992; Velbel, 1993). Differences in rates can be contrasted by comparing residual mineral abundances in the Merced soils (Fig. 2B) with abundances predicted by the simple geometric model expressed by Equation (17) (Lasaga, 1984). An experimental k_j=-16.0 mol cm^{-2} s^{-1} for albite (Table 7) predicts a residence time of 575k yr for a 1 mm diameter grain. Yet >50% of a comparable size fraction of plagioclase persists in the Turlock Lake soil after 600 kA (Fig. 2B). An experimental k_j = -16.5 mol $cm^{-2}.s^{-1}$ predicts that K-feldspar would persist for 920 kyr and yet >20% of the K-feldspar remains in the China Hat soil after 3000 kA (Fig. 2B). These discrepancies between experimental and natural rates are based on extremely conservative estimates. If the average roughness for crushed feldspar used in the dissolution experiments were introduced into the geometric model ($\lambda \approx 8$; Blum, 1994), the residence times for the feldspars would be reduced to 35 to 70 kA. If the surface areas comparable to actual weathered silicates were used (λ >100), the model would produce extremely unrealistic residence times of <10 kA.

These apparent discrepancies in magnitude of the rate constants signify either that significant variability must exist in the approaches and methodologies used to calculate the rate constants and/or that significant variability must exist in fundamental processes which control dissolution kinetics in natural and experimental systems. The following sections present a brief review of probable causes of such variability. Additional discussions on the relative rates of experimental and natural systems are given by Sverdrup (this volume).

Surface area

Variation in the rate constants tabulated in Table 7 can be attributed, in part, to differences in normalizing the solid or solute flux relative to unit surface area of mineral surface (Eqn. 1). As indicated in Table 7, rate constants for weathering in natural systems have employed both geometric or BET estimates of surface areas. Indeed there has been a tendency in the literature to use these two approaches interchangeably in comparing weathering rates. Due to natural surface roughness, BET surface areas are generally 2 to 3 orders of magnitude greater than geometric estimates of surface area. As indicated for the

weathering study on the Merced chronosequence, the geometric surface area model produces dissolution rates that are 10^2 to 10^3 orders of magnitude faster than the variable-roughness model (Fig. 13).

In contrast to natural systems, experimental studies have almost exclusively utilized BET surface area measurements. Therefore, differences in surface area estimates do not explain why the experimental rates are significantly faster than natural rates. In fact if many of the reported natural rates, based on geometric surface areas estimates, were renormalized using realistic values of surface roughness, the apparent discrepancies with experimental rates would even be greater. Therefore, other processes, representing fundamental controls on chemical weathering rates, must be also responsible for the discrepancies apparent in Table 7.

Soil age

Several lines of evidence suggest that mineral weathering rates decrease with time. In terms of a total soil, exponential decay in rates (Fig. 2) can be attributed to decreases in weatherable aluminosilicates relative to residual phases such as quartz. Slower weathering rates in the Merced chronosequence can be attributed to the greater age of most of these soil profiles relative to most other studies which have considered weathering in areas glaciated during the Pleistocene (~10 kA). However, other evidence indicates that the dissolution rate constants for individual aluminosilicate minerals may also decrease with time The Merced study is the first time that weathering rates for individual minerals have been documented to decrease with time (White et al., 1995). As shown in Figure 13, rate constants for plagioclase, K-feldspar and hornblende calculated from BET surface areas decrease by more than an order of magnitude over 3 million years of weathering.

Decreases in weathering rate constants with time can be explained, in part, by the decoupling of the direct proportionality between physical surface areas and the density of reaction sites with increasing time. On an atomistic level, heterogeneity in surface energies is expected to decrease as reaction sites at compositional impurities, dislocations and other crystallographic defects are selectively reacted (Brantley et al., 1986; Blum and Lasaga, 1987). Therefore, the reactivity per unit of physical surface area may decrease. Rates for minerals with high-energy heterogeneities are expected to be initially very rapid as reactive material is removed from etch pits. Rates will then decrease significantly after these sites are depleted and less reactive sites dominate. In contrast, minerals with initially less surface energy heterogeneity would be expected to exhibit a less pronounced decrease in dissolution rate with time. Larger decreases in reaction rates with time for minerals with higher potential surface heterogeneity are suggested for the Merced soils (White et al., 1995). In the A horizon, for example, hornblende weathering rates appears to decrease by a factor of about 45 between 10 kA and 3000 kA, plagioclase by a factor of ~16 and K-feldspar by ~4.5, the same order as decreasing etch pits abundance observed by SEM (Fig. 10).

BET measurements on primary silicates from soils have generally been performed on clean surfaces from which adhering clay and Fe oxyhydroxide layers were removed (White and Peterson, 1990; Anbeek, 1992; White et al., 1995). Increasing concentrations of these secondary phases in soils of increasing age may also exert a negative impact on dissolution rates by effectively shielding chemical interaction between the physical mineral surface and soil waters. This scenario is supported by the observation that with increasing age, the measured BET surface areas of the untreated bulk soils become progressively less than the sum of the separated Fe hydroxides, clays, and primary silicate components (White et al., 1995). This implies that in untreated soils, components such as Fe oxyhydroxides, are occluding the gas absorption and by inference, aqueous interaction in the soil environment.

Solute chemistry

Soil solute chemistry is both produced by and may influence weathering reactions in soils. Solution pH has been shown to be a significant factor in controlling experimental silicate dissolution rates (see Blum and Stillings and Brantley, this volume). This is because both H^+ and OH^- are important participants in dissolution mechanisms, and fluctuate more widely in concentration than any other natural solute. Except in the case of strong acidification [Swoboda-Colberg and Drever, 1992], the reported pH of soil and catchment waters generally range between 4 to 8. In reviewing dissolution of plagioclase and K-feldspar, Blum (1994) (also see Blum and Stillings, this volume) showed dissolution rates are at minimum constant values between pH 5 and 8. Below approximately pH 5, the rate constant for feldspars becomes proportional to $[H^+]^{0.5}$ This data suggest that weathering rates change by a factor of 5 between pH 4 and 5, a pH range typical of acid soils. A variation in solution input pH of 4.5 to 4.0 during artificial acidification of soils at Bear Brook, Maine (Swoboda-Colberg and Drever, 1992). produced a factor of 3 increase in rate constant (k_f = $7.8x10^{-18}$ to $2.0x10^{-17}$ mol.cm^{-2}.s^{-1}) for reactive minerals dominated by plagioclase and mica. However for soils in the more neutral pH range, weathering rates are not particularly sensitive to pH changes.

As previously discussed (Eqn. 31), soil solute compositions impact soil weathering rates via reaction affinity. Burch et al. (1993) investigated the effects of approach to equilibrium from undersaturation on the rates of albite dissolution at pH 8.8 and 80 °C. At $\Delta G_r \geq$ -10 kcal, dissolution rates were independent of saturation state. The rates of dissolution decreased rapidly in the range of -10 to -7 kcal and reached a plateau from ΔG_r of -7 to close to equilibrium. Based on Figure 19, ΔGr for most soil solutions at pH ≥ 5 are in excess of -10 kcal with respect to albite (Fig. 19). Assuming that the experimental ranges (Burch et al., 1993) can be extrapolated to ambient soil temperatures, the saturation state of most soils waters should strongly affect albite dissolution rates. Although no experimental data is available on the effects of ΔG_r on K-feldspar dissolution, soil solutions are generally closer to saturation than for albite (Fig. 19) and therefore the K-feldspar rates may be even more retarded in soil solutions. This effect has been suggested by Brantley et al. (1995) as the reason for why K-feldspar apparently weathers at a slower rate in field conditions relative to albite.

In addition, thermodynamic saturation, the concentration of specific aqueous species in soil solutions may also impact mineral dissolution rates. Oelkers et al. (1994) showed at elevated temperatures (150°C) increasing Al concentrations decreased reaction rates far from equilibrium. This effect was attributed to the presence of a reactive surface precursor that does not have the same Al:Si stoichiometry as the original silicate mineral. Studies have also documented that the addition of aqueous SiO_2 retards the dissolution of kaolinite in alkaline solutions far from equilibrium (Devidal et al., 1992). This is likely the result of adsorption of aqueous silica which adds cross links to the silica network forming silanol groups. As suggested by the above discussion, specific soil water chemistry can influence weathering rates of minerals in complex ways. For example, although decreasing pH will accelerate weathering rates, concurrent increases in Al release will tend to concurrently retard dissolution. As pointed by Sverdrup (1990) (also see Sverdrup, this volume), an rigorous approach to quantitatively modeling weathering reactions requires the ability to simultaneous consider this solution effects.

Hydrologic heterogeneity

Heterogeneity in soil zone hydrology impacts soil solution chemistry, fluid residence

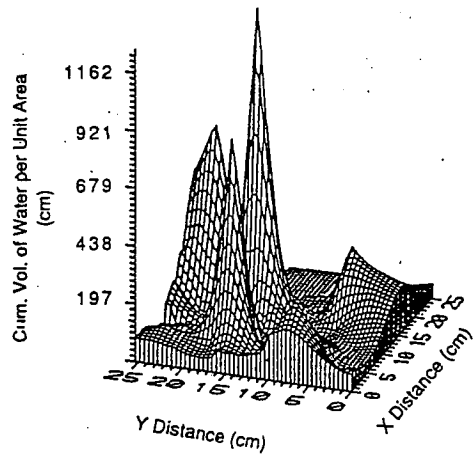

Figure 22. Soil hydrologic heterogeneity as demonstrated by variations in cumulative volume of water that has flowed through sections of an *in situ* soil column (after Andreini and Steenhuis, 1993).

times, and effective mineral surface areas exposed to weathering reactions. Formation of duripans or fragipans, which significantly retard the movement of water and solutes through the soil zone, is reviewed by Smeck and Ciolkosz (1989) and Nettleton (1991). The effect of SiO_2 fragipan formation on soil moisture content, matrix potential and solute chemistry is demonstrated for Riverbank soil profile (Fig. 21).

In contrast, preferential flow can be generated by soil macropores generated from plant roots, burrowing animals, soil cracks and sedimentological heterogeneity (Gish and Shirmohammadi; 1991). An example of preferential flow due to macropores is shown in Figure 22 for the rates of fluid flux through the cross sectional area of a large scale field lysimeter (Andreni and Steenus, 1993). Such preferential flow, which can increase fluid fluxes by an order of magnitude, will also decrease the fluid residence time and thus decrease soil solution concentrations and reaction affinities.

If a large fraction of the mobile fluid interacts with a small proportion of the potentially available mineral surface area , rates calculated from total soil surface area will significantly underestimate the natural weathering rate (Velbel, 1993). In addition, if soil lyimeters predominantly sample matrix pore water, the corresponding high solute concentrations will overestimate solute fluxes which in reality are dominated by lower solute concentrations associated with macropore flow. Several researchers suggested soil heterogeneity is responsible for the apparent lower weathering rates in natural systems relative to experimental studies (Swoboda-Colberg and Drever, 1992; Velbel, 1993).

Role of biological activity

The role of plants and associated mirco-biota in chemical weathering has received intense recent interest in relation weathering and the earths' climate (Berner, this volume). Most data collected to date on the effects of plants on silicate weathering have been descriptive and generally inconclusive (Huang and Schnitzer, 1986). Potential influences of plants on chemical weathering in soils include effects of pH, organic ligands and issues related to physical and hydrologic processes, such as erosion, moisture retention and transpiration (Drever,1994).

Plant root respiration impacts soil water pH through the release of CO_2. P_{CO2} is

commonly 1 to 2 orders of magnitude higher than atmospheric CO_2 (P_{CO2} =$10^{-3.5}$ atm). Plant CO_2 respiration is the main source of H^+ which drives the silicate hydrolysis reaction responsible for soil weathering. However due to associated buffering reactions, even very high P_{CO2} values will not generate soil pHs in excess of 4.5. As previously indicated, reaction rates at or above these pHs probably do not vary by more than a factor of 2 or 3. Organic acids produced by biological activity can also depress soil solution pH. However, these species are not present in most soil solutions at concentrations sufficient to significantly lower the pH to a degree which can accelerate weathering reactions (Drever, 1994).

Organic ligands produced by biological activity influence soil weathering rates by complexing with the species such as Al on silicate surfaces and thus facilitate breaking of the structural bonds and accelerating weathering. In contrast, the sorption of non-complexing organics on to mineral surfaces may decrease dissolution rates by effectively shielding the reactive surface from proton-induced reactions. Most experimental studies to date have focused on dissolution involving strong complexing ligands such as oxalate at concentrations significantly higher than that measured in soil waters. Even these results suggest that complexation does not increase silicate dissolution rates by more than a factor of 2 to 3 (Welch and Ullman, 1993).

Field data, in contrast, suggests that vegetation can significantly affect chemical weathering. Conifer forest plantations impact soil acidity and the release of Al and other species from soil exchange and weathering of soils (Huges et al., 1994). In a recent paper, Cochran and Berner (1995) (see Berner, this volume) showed that vascular plants augment chemical weathering by at least an order of magnitude relative to abiotic conditions. These and other results suggest that such accelerated weathering occurs in micro-environments associated with roots and fungal hyphae where pH and organic ligands may be significantly more concentrated than measured in soil water.

Climate

The origin of the term "weathering" implies that chemical weathering in soils is strongly affected by climate, principally by moisture and temperature. Moisture is influenced by the total amount, intensity, and seasonality of precipitation, humidity, evapo-transpiration, runoff and infiltration. Thermal effects include average air temperatures, seasonal temperature variations, and thermal gradients in soils. Changes in these climatic parameters are expected to impact chemical weathering.

The most simplistic description of the effect of temperature on chemical reaction rates is the Arrhenius relationship. The ratio of rate constants k_j and k_j° at temperatures T and T° (°K), respectively, can be predicted by the expression

$$\frac{k_j}{k_j^\circ} = \exp\left[\frac{E_a}{R}\left(\frac{1}{T^\circ}-\frac{1}{T}\right)\right] \qquad (38)$$

where R is the gas constant factor and E_a (kJ mol^{-1}) is the reaction activation energy.

Figure 23 indicates that increases in activation energy increases the temperature effect on weathering rates. Experimental studies generally report activation energies for silicate minerals ranging between 30 and 90 kJ mol^{-1} (Knauss and Wolery, 1986; Sverdrup, 1990; Brady and Carroll, 1994) (see present volume). As pointed out by Velbel (1990), the exponential character of the Arrhenius equation can produce strong non-linear effects on

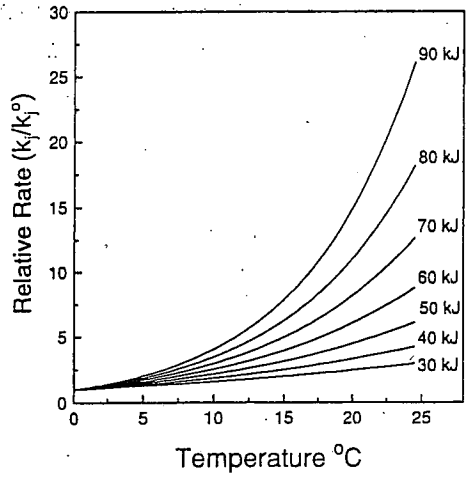

Figure 23. Relationship between ratios of reaction rate constants k_j and k_j^o and temperatures T^o = 0°C and T for activation energies ΔG_r between 30 and 90 kJ.

weathering due to temperature variations in shallow soils. For example, short periods of relatively warm temperatures will have a disproportionate effect on weathering rates relative to long periods of cool temperatures.

Water content also has long been considered an important parameter in soil development but has only recently been considered in terms of weathering mechanisms (Swoboda-Colberg and Drever, 1992; Velbel, 1993). Increasing precipitation, moisture, and solvent throughput can affect the unsaturated hydrology of the soil zone, and accelerate weathering rates by increasing the wetted surface areas of minerals. In addition, as soils become wetter, stagnant pore waters, that are immobile under drier conditions, become hydrologically connected and can potentially activate weatherable mineral surfaces. Areas of high precipitation also generally correlate with areas of greater vegetative cover which can influenced weathering processes as previous discussed. In contrast, low rates of precipitation and/or high rates of *ET* will produce more concentrated soil solutions that will be thermodynamically closer to mineral equilibrium than in wetter soils. High solute concentrations may also promote the effects of Al and other species that have been experimentally shown to inhibit feldspar dissolution

Based on watershed fluxes, linear relationships between weathering and annual average precipitation and runoff have been developed (Dethier, 1986). Recently White and Blum (1995b) proposed a coupled relationship

$$Q_w = (a_1 * P) \exp\left[-\frac{E_a}{R}\left(\frac{1}{T}-\frac{1}{T_o}\right)\right] \tag{39}$$

in which the chemical flux Q_w varied as the product of a linear precipitation term P and an exponential temperature term (Eqn. 38). Equation (39) predicts that the effect of precipitation on weathering is much greater in regions of higher temperatures than in regions of lower temperatures. Conversely, the temperature function is dependent on precipitation. For weathering exposed to low precipitation, the apparent exponential effect of temperature on weathering will be quite low. For wet regions, the exponential influence of temperature on weathering becomes very pronounced. The net effect of the above relationship is to reinforce

weathering in areas of both high temperature and precipitation as in the tropics and to decrease weathering fluxes in watersheds with low temperature and precipitation such as in the arctic. At present, this model has been calibrated on a watershed scale and not yet been validated in terms of actual weathering rates in soil environments.

CONCLUSION

Although the subject of chemical weathering in soils has been the focus of extensive research over the last century, surprisingly meager information is available on quantitative weathering rates of primary silicates in soil environments. This paper documents approaches employed to obtain such rates, summarizes available data, and identifies chemical, physical, and hydrologic processes responsible for the observed variability.

Silicate weathering rates are addressed from several perspectives. Changes in mineral masses during soil formation require determination of initial and final compositions of both weatherable silicates and inert elements or minerals in the soil. Approaches are demonstrated for calculating weathering velocities in saprolite profiles and in documenting the effects of climate on rates of soil development. Use of soil solute fluxes in calculating mineral weathering rates involves solving mass balances which relate the array of solute species to dissolution and precipitation of specific mineral phases. Solute mass fluxes require the determination of the fluid flux through the soil, based on either estimates of hydraulic conductivity or on input/output balances for conservative tracers such as chloride.

Calculation of weathering rates requires normalization of mass balances to specific mineral surface areas. Approaches to surface area characterization include macroscopic geometric estimates and microscopic BET measurement. Surface areas determined from these approaches progressively diverge as mineral surfaces roughen and porosity increases with weathering intensity.

Weathering rates, derived from mineral mass balances and solute fluxes, are compared for a Merced soil profile, and found to be similar. This agreement is remarkable considering the number of assumptions used and the fact that the mineral balance approach integrates weathering over the entire time of soil development while the solute approach is based on fluid residence times of several years. However reported rates of specific minerals weathering under both natural and experimental conditions where found to vary between 3 and 4 orders of magnitude. This range is greater than difference in rates between minerals. Such variations are caused, in part, by differing approaches used to calculate rate constants, particularly in regard to surface areas.

Other reasons for variations in rate constants are attributable to fundamental processes which impact weathering reactions in the natural environment. These include the effects of soil age on mineral surface reactivity, the role of hydrologic heterogeneity on fluid residence time and reactive mineral surfaces, the effects of soil solution pH, speciation and reaction affinities, and finally the impact of vegetation and climate. In summary this paper outlines the quantitative framework by which soil weathering rates can be calculated and compared. Clearly much additional work is required to understand the geochemical processes that impact the results generated by these approaches.

ACKNOWLEDGMENTS

Recognition is given to numerous colleagues who provided important insights into the role of chemical weathering in soil environments. These include Alex Blum, Tom Bullen, Marjorie Schulz, Jennifer Hardin and David Stonestrom at the U.S. Geological Survey and

Susan Brantley at Pennsylvania State University. Additional field data and support was provided by Matt Larsen in San Juan, Puerto Rico and Tom Huntington in Atlanta, Georgia. This effort was supported by the Global Change Program at the U.S. Geological Survey.

REFERENCES

Allison GB, Gee GW, Tyler SW (1994) Vadose zone techniques for estimating groundwater recharge in arid and semiarid regions. Soil Science Am J 58:6-14

Anbeek C (1992) Surface roughness of minerals and implications for dissolution studies. Geochim. Cosmochim. Acta 56:1461-1469

Anbeek C Van Breemen N, Meijer EL, Van Der Plas L (1994) The dissolution of naturally weathered feldspar and quartz. Geochim Cosmochim Acta 58:4601-461

Andreneni MS and Steenhuis TS (1993) Role of soil heterogeneity in macropore flow. J Hydrol 143:79

April R, Newton R, Coles LT (1986) Chemical weathering in two Adirondack watersheds: Past and present-day rates. Geol Soc Am Bull 97:1232-1238

Arocena JM, Pawluk S, Dudas MJ (1994) Mineral transformations in some sandy soils from Alberta, Canada. Geoderma 61:17-38

Bain DC, Mellor A, Roberston-Rintoul MS, Buck, ET (1993) Variations in weathering processes and rates with time in a chronosequence of soils from Glen Feshie, Scotland. Geoderma 57:275-293

Bateman PC, and Chappell BR. (1979) Crystallization, fractionation, and solidification of the Tuolumne Intrusive Series, Yosemite National Park, California Geol Soc Am Bull 90: 465-482

Barth TF (1961) Abundance of the elements, aerial averages and geochemical cycles. Geochim Cosmochim Acta 23:1-8

Berner RA, Holdren GR (1979) Mechanism of feldspar weathering- II. Observations of feldspar from soils. Geochim Cosmochim Acta 43:1173-1186

Berner RA, Sjoberg EL, Vebel MA, Kromand DM (1980) Dissolution of pyroxenes and amphiboles during weathering. Science 207:1205-1206

Birkeland PW (1984) Soils and Geomorphology, Oxford University Press, 372 p

Blum AE (1994) Feldspars in weathering. In: Parsons, I (ed) Feldspars and Their Reactions. Kluwer-Academic Press, Netherlands p 595-629

Blum AE, Lasaga AC (1987) Monte Carlo simulations of surface reaction rate laws. In: Stumm W (ed) Chemical Processes at the Particle-Surface Interface. Wiley and Sons, New York, p 255-291

Brady PV, Carroll SA (1994) Direct effects of CO_2 and temperature on silicate weathering: possible implications for climate control. Geochim Cosmochim Acta 58:1853-1863

Brantley SL, Crane SR, Hellimann R, Stallard R (1986) Dissolution at dislocation etch pits in quartz. Geochim Cosmochim Acta 50:2349-2361

Brantley SL, Blai AC, Cremeens DL, MacInnis I, Darmody RG (1993) Natural etching rates of feldspar and hornblennde Aquatic Sci 55:262-272

Brantley SL, Richards P, Murphy S (1995) Soil porewater chemistry and the relative rate of weathering of feldspar and quartz. Geochim. Cosmochim. Acta (in review)

Brimhall G, Dietrich WE (1987) Constitutive mass balance relations between chemical composition, volume, density, porosity, and strain in metasomatic hydrochemical systems: Results on weathering and pedogenesis. Geochim Cosmochim Acta 51: 567-587

Buol W. Hole FD, McCracken RJ (1989) Soil Genesis and Classification. Iowa State University Press, Ames Iowa, 453 p

Buol S, Weed SB (1991) Saprolite-soil transformations in the Piedmont of North Carolina. Geoderma 51:15-28

Burch TE, Nagy KL, Lasaga AC (1993) Free energy dependence of albite dissolution kinetics at 80°C, and pH 8.8. Chem Geol 105:137-162

Busacca AJ, Singer MJ (1989) Pedogensis of a chronoseqence in the Sacramento Valley, California, U. S. A., II. Elemental chemistry of silt fractions. Geoderma 44: 43-75

Busacca AJ, Singer MJ, Verosub KL (1989) Late Cenozoic stratigraphy of the Feather River, Yuba Rivers area, California with a section on soil development in mixed alluvium at Honocut Creek. U. S. Geol Surv Professional Paper 1590:131 p

Campbell DJ, Kinniburgh, DG, Beckett PHT (1989) The soil solution chemistry of some Oxfordshire soils: temporal and spatial variability. J Soil Science 40:321-339

Chadwick OA, Brimhall GH, Hendricks DM (1990) From black box to a grey box: a mass balance interpretation of pedogensis. Geomorphology 3:369-390

Claassen HC, White AF (1979) Application of geochemical kinetic data to groundwater systems, Part I. A tuffaceous-rock system in southern Nevada. In: Jenne E (ed) Am Chem Soc Symp Ser 93:447-473

Cleaves ET (1993) Climatic impact on isometric weathering of a coarse-grained schist in the northern Piedmont Province of central Atlantic states. Geomorphology 8:191-198

Chou L, Wollast, R (1984) Study of the weathering of albite at room temperature and pressure with a fluidized

bed reactor. Geochim Cosmochim Acta 48:2205-2217
Cochran MF, Berner RA (1995) Promotion of chemical weathering by higher plants: field observations on Hawaiian basalts. Chem Geol (in press)
Cremeens DL, Darmody RG, Norton LD (1992) Etch-pit size and shape distribution on orthoclase and pyriboles in a loess catena. Geochim Cosmochim Acta 56: 3423-3434
Cronan C, Driscoll C, Newton RM, Kelly M, Schofield CL, Bartlett RJ, April R (1990) A comparative analysis of aluminum biogeochemistry in a Northeastern and a Southeastern forested watershed. Water Resources Res 26:1413-1430
Dethier DP (1986) Weathering rates and the chemical flux from catchments in the Pacific Northwest, U.S.A. In: Coleman S, Dethier DP (eds) Rates of Chemical Weathering of Rocks and Minerals. Academic Press, Orlando, p 503-530
Devidal JL, Dandur JL, Schott J (1992) Dissolution and precipitation kinetics of kaolinite as a function of chemical affinity (T = 150°C, pH 2 and 7.8) In: Kharaka Y, Maste A (eds) Water Rock Interaction 7, Balkema. p 93-96
Dixon JB, Weed JB (1989) Minerals in Soil Environments. Soil Sci Soc Am Ser 1 893 p
Drever JI (1994) The effect of land plants on weathering rates of silicate minerals. Geochim Cosmochim Acta 58:2325-2332
Edmeades DC, Wheeler DM, Clinton OE (1985) The chemical composition and ionic strength of soil solutions from New Zealand top soils. Aust J Soil Res 23:151-165
Erikkson E, Kunakasem V (1969) Chloride concentrations in groundwater, recharge rate and rateofdeposition of chloride in the Israel coastal plain. J Hydrology 7:178-197
Feller E, Schoulle E, Thomas F, Roiller J, Herbillon A (1992) N_2 BET surface areas of some low activity soils and their relationships with secondary constituents and organic matter. Soil Sci 153:279-299
Flury M, Fluhler H, Jury WA, Leuberger J (1994) Susceptibility of soils to preferential flow of water: A field study. Water Resources Res 30:1945-1954
Gallez A, Juo ASR, Herbillion AJ (1976) Surface charge characteristics of selected soils in the tropics. Soil Sci Soc Am J. 40:601-608
Garrels RM, Christ CL (1965) Solutions, Minerals, and Equilibrium. Freeman, Cooper, San Francisco, 395 p
Gish TJ, Shirmohammadi A (1991) Preferential Flow. Proc. Nat. Symp, Chicago, IL, Am Soc of Agricultural Engineers, 525 p
Globus AM, Gee, GW (1995) Method to estimate water diffusivity and hydraulic conductivity of moderately dry soil. Soil Sci Soc Am J 59:684-689
Goldich SS (1938) A study in rock-weathering. J Geol 46:17-53
Hall RD, Horn LL (1993) Rates of hornblende etching in soils in glacial deposits of the northern Rocky Mountains (Wyoming-Montana, USA): Influence of climate and characteristics of the parent material. Chem Geol 105:17-19
Hall RD, Martin RE (1986).The etching of hornblende grains in the matrix of alpine tills and periglacial deposits. In: Colman S, Dethier D (eds.) Rates of Chemical Weathering of Rocks and Minerals. Academic Press, Orlando, p 101-128
Harden JW (1987) Soils developed in granitic alluvium near Merced, California. U.S. Geo Surv Bull 1590-A, 129 p
Helgeson HC, Murphy WM, Aagard P (1984) Thermodynamic and kinetic constraints on reaction rates among minerals and aqueous solutions, II. Rate constants and effective surface area, and the hydrolysis of feldspar. Geochim Cosmochim Acta 48:2405-2432
Hem JD (1985) Study and interpretation of the chemical characteristics of natural water. U.S. Geol Surv Water Supply Paper 2254:264 p
Hillel D (1982) Introduction to Soil Physics., Academic Press San Diego, 329 p
Hillel D, Gardner WR (1970) Measurement of unsaturated conductivity diffusivity by infiltration through an impeding layer. Soil Sci 109:149-154
Holdren Jr GR, Speyer P (1987). Reaction rate-surface area relationships during the early stages of weathering. II. Data on eight additional feldspars. Geochim Cosmochim Acta 51:2311-2318
Huang PM, Schnitzer M. (1986) Interactions of Soil Minerals with Natural Organics and Microbes. Soil Sci Am Spec Publ.17, 529 p
Huges S, Norris DA, Reynolds B, Williams TG (1994) Effects of forest age on surface drainage and soil solution aluminum chemistry in stagnopodzols in Wales. Water, Air, Soil Pollut 77:115-139
Jaycock MJ Parfitt GD (1981) Chemistry of Interfaces, Ellis Horwood, New York, 329 p
Jenny H (1980) Factors of Soil Formation. McGraw-Hill, New York, 239 p
Joffe JS (1933) Lysimeter studies. 2. The movement and translocation of soil constituents in the soil profile. Soil Sci 35:239-257
Joffe JS (1949) Pedology. Pedological Publications, New Brunswick, N J 2nd Ed, 239 p
Johnsson MJ, Ellen SD, McKittrick MA (1993) Intensity and duration of chemical weathering: An example from clays of southeastern Koolau Mountains, Oahu, Hawaii. Geol Soc Am Spec Paper 284:147-169
Karathanasis AD (1989) Solution chemistry of fragipan formation, thermodynamic approach tounderstanding

fragipan formation. In: Smeck NE, Ciolkosz EJ (eds) Fragipans: Their Occurrence, Classification and Genesis. Soil Sci Am. Spec. Publ 24:113-141
Katz BG.(1989) Influence of mineral weathering reactions on the chemical composition of soil water, springs, and groundwater, Catoctin Mountains, Maryland. Hydrol Processes 3:185-202
Kenoyer GJ, Bowser C (1992) Groundwater evolution in a sandy silicate aquifer in Northern Wisconsin 1. Patterns and rates of change. Water Resources Res 28:579-589
Kharaka YK, Gunter WD, Aggarwal PK, Perkins E, Debraal JD (1988) SOLMINEQ 88: A computer program for geochemical modeling of water-rock interactions. U. S. Geol Surv Water Resources Invest Rept 88-4227, 419 p
Knauss, KG, Wolery TJ (1986).Dependence of albite dissolution kinetics on pH and time at 25°C and 70°C. Geochim Cosmochim Acta 50:2481-2497
Lasaga AC (1981) Transition state theory. In: Lasaga, AC, Kirkpatrick, RJ (eds.) Kinetics of Geochemical Processes. Reviews Mineral 8:135-169 p
Lasaga AC (1984) Chemical kinetics of water-rock interaction. Geophys Res 89:4009-4025
Lasaga AC, Soler JM, Ganor J, Burch TE, Nagy KL (1994) Chemical weathering and global chemical cycles. Geochim Cosmochim Acta 58:2361-2386
Leamnson RN, Thomas Jr. J, Ehrlinger HP (1969) A study of the surface areas of particulate microcrystalline silica and silica sand. Illinois State Geol Surv Cir 444:12 p
Lindsay W (1979). Chemical Equilibria in Soils. John Wiley and Sons, New York, 395 p
Locke WW (1986) Rates of hornblende etching in soils on glacial deposits, Baffin Island, Canada. In: Coleman S, Dethier, D (eds.) Rates of Chemical Weathering of Rates and Minerals. Academic Press, Orlando, p 129-146
MacInnis IN, Brantley SL (1993) Development of etch pit size distributions on dissolving minerals. Chem Geol 105:31-49
Mahaney WC, Halvorson DL (1986) Rates of mineral weathering in the Wind River Mountains, western Wyoming. In: Coleman, S, Dethier, D.(eds.) Rates of Chemical Weathering of Rates and Minerals. Academic Press, Orlando, p 147-168
Manley EP, Chesworth W, Evans LJ (1987) The solution chemistry of podzolic soils from the eastern Canadian shield: A thermodynamic interpretation of the mineral phases controlling soluble Al^{3+} and H_4SiO_4. J Soil Sci 38:39-51
Merrill G.P (1906). A Treatise on Rocks, Rock Weathering and Soils. MacMillian, New York, 389 p
Merritts DJ, Chadwick OA, Hendricks DM, Brimhall GH, Lewis CJ (1992) The mass balance of soil evolution on late Quaternary marine terraces, Northern California. Geol Soc Am Bull 104:1456-147
Montgomery CW, Brace WF (1975) Micropores in plagioclase. Contrib Mineral Petrol.52:17-28.
Nagy KL, Lasaga AC (1993) Simultaneous precipitation kinetics of kaolinite and gibbsite at 80°C and pH 3. Geochim Cosmochim Acta 57:4329-4335
Nagy KL, Blum AE, Lasaga AC (1991) Dissolution and precipitation kinetics of kaolinite at 80°C and pH 3: The dependence on the saturation state. Am J Sci 291:649-686
Nahon DB (1991) Introduction to the Petrology of Soils and Chemical Weathering. John Wiley and Sons, New York, 429 p
Nettleton WD (1991) Occurrence, Characteristics and Genesis of Carbonate, Gypsum, and Silica Accumulations in Soils. Soil Sci Soc Am. Spec Publ 26, 149 p.
Norfleet ML, Karathanasis AD, Smith BR (1993) Soil solution composition relative to mineral distribution in the Blue Ridge Mountain soils. Soil Sci Amer J 57:1375-1380
Oelkers EH, Schott J, Devidal JL (1994) The effect of aluminum, pH and chemical affinity on the rates of alumino-silicate dissolution reactions. Geochim Cosmochim Acta 58:2011-2024
Oxburgh R, Drever, JI, Sun YT (1994) Mechanism of plagioclase dissolution in acid solutions at 25°C. Geochim Cosmochim Acta 58:661-669
Paces T (1983) Rate constants of dissolution derived from the measurement of mass balance in hydrologic catchments. Geochim Cosmochim Acta 47: 1855-1863
Parkhurst DL, Plummer LN, Thorsten DC (1982) BALANCE-A computer program for calculating mass transfer for geochemical reactions in groundwater. U.S. Geol Surv Water Resources Invest 82-14, 29 p
Parks GA (1990) Surface energy and adsorption at mineral-water interfaces: An introduction. In: Hochella Jr MF, White AF (eds) Mineral-Water Interface Geochemistry, Reviews Mineral 23:133-169
Pavich MJ, Brown L, Harden J, Klein J, Middleton R (1986) ^{10}Be distribution in soils from Merced River terraces, California. Geochim Cosmochim Acta 50:1727-1735
Plummer LN, Presterson EC, Parkhurst DL (1991) An interactive code (NETPATH) for modeling NET geochemical reactions along a flow path. U.S. Geol Surv Water Resources Invest Rept 91-4078, 277 p
Reynolds B, Neal C, Hornung M, Hughs S, Stevens PA (1988) Impact of afforestation on the soil solution chemistry of stagnopodzols in Mid-Wales. Water, Air, Soil Pollut 38:55-70
Richards LA (1931) Capillary conduction of liquids in porous media. Physics 1: 318-333
Schnoor JL (1990) Kinetics of chemical weathering: A comparison of laboratory and field rates. In: Stumm W (ed) Aquatic Chemical Kinetics, John Wiley and Sons, New York, p 475-50

Schweda P (1989) Kinetics of alkali feldspar dissolution at low temperature Proc. 6th Internat. Symp. Water/Rock Interaction, A.A. Balkema, Rotterdam, p 609-612
Siegal DI, Pfannkuch HO (1984) Silicate dissolution influence on Filson Creek chemistry, northeastern Minnesota. Geol Soc Amer Bult 95:144-1453
Smeck NE, Ciolkosz EJ (1989) Fragipans: Their Occurrence, Classification and Genesis. Soil Sci Amer Spec Publ 24, 153 p
Soulsby C, Reynolds B (1992) Modeling hydrological processes and aluminum leaching in an acid soil at Lyn Brianne, Mid-Wales. J Hydrology 138:409-429
Sparks DL, Suarez DL (1991) Rates of Soil Chemical Processes. Soil Sci Am Spec Publ. 27, 329 p
Sposito G (1994) Chemical Equilibria and Kinetics in Soils. Oxford Press, New York, 423p
Sverdrup H (1990) The Kinetics of Base Cation Release Due to Chemical Weathering. Lund University Press, Lund, Sweden 346 p
Sverdup H, Warfvinge F (1988) Weathering of primary silicate minerals in the natural soil environment in relation to a chemical weathering model. Water, Air, Soil Pollut.38:387-408
Swoboda-Colberg NG, Drever JI (1992) Mineral dissolution rates: A comparison of laboratory and field studies Proc. 7th Int. Symp Water Rock Interaction. Park City, Utah, Balkema, Rotterdam, p 115-117
Ugolini FC, Dahlgren R, Shoji S, Ito T (1988) An example of podzolization as revealed by soil solution studies, southern Hakkoda, Northeastern Japan. Soil Sci 145:111-125
Velbel MA (1985) Geochemical mass balances and weathering rates in forested watersheds of the southern Blue Ridge. Am J Sci 285:904-930
Velbel MA (1986) The mathematical basis for determining rates of geochemical and geomorphic processes in small forested watersheds by mass balance: Examples and implications. In: Colman S, Dethier D (eds) Rates of Chemical Weathering of Rocks and Minerals. Academic Press, Orlando, p 439-448
Velbel MA (1989) Weathering of hornblende to ferruginous products by a dissolution-reprecipitation mechanism: petrography and stoichiometry. Clay Clay Minerals 37:515- 524
Velbel MA (1990) Influence of temperature and mineral surface characteristics on feldspar weathering rates in natural and artificial systems: a first approximation. Water Resources Res 25:3049-3053
Velbel MA (1993) Constancy of silicate-mineral weathering-ratios between natural and experimental weathering: Implications for hydrologic control of differences in absolute rate. Chem Geol 105:89-99
Wakatsuki T, Rasyidin A (1992) Rates of weathering and soil formation. Geoderma 52:251-263
Welch SA, Ullman WJ (1993) The effect of organic acids on plagioclase dissolution rates and stoichiometry. Geochim Cosmochim Acta 57:225-2736
Wesolowski D J (1992) Aluminum speciation and equilibrium in aqueous solution: I. the solubility of gibbsite in the system NA-K-Cl-OH-Al(OH)$_4$ from 0 to 100°C. Geochim Cosmochim Acta 56:1065-1091
White AF, Peterson ML (1990) Role of reactive surface area characterization in geochemical models. Chemical modeling of aqueous systems II, In: Melchior DC, Bassett RL (eds) Am Chem Soc Symp Ser 416, p 461-475
White AF, Blum AE (1995a) Climatological influences on chemical weathering in watersheds; application of mass balance approaches. In: Trudgill S (ed) Solute Modeling in Catchment Systems. John Wiley, New York, (in press)
White AF, Blum AE (1995b) Effects of climate on chemical weathering rates in watersheds. Geochim Cosmochim Acta 59:1729-1747
White AF, Blum AE, Schulz MS, Bullen TD, Harden JW, Peterson ML (1995) Chemical weathering of a soil chronosequence on granitic alluvium 1: Reaction rates based on changes in soil mineralogy. Geochim Cosmochim Acta (in press)
Willaime C, Christie JM, Kovacs MP (1979) Electron microscope study of plastic defects in experimentally deformed alkali feldspars. Bull. Soc fr Mineral Cristallogr 100:263-271
Wood WW, Kraemer TF, Hearn PP (1990) Intergranular diffusion: An important mechanism influencing solute transport in clastic aquifers. Science 247:1596-1571
Worden RH, Walker FD, Parsons I, Brown WL (1990) Development of microporosity, diffusion channels and deuteric coarsening in perthitic alkali feldspars. Contrib Mineral Petrol 104:507-515
Zhang H, Bloom PR, Nater EA (1993) Changes in surface area and dissolution rates during hornblende dissolution at pH 4.0. Geochim Cosmochim Acta 57:1681-1689